A comparison of ozone measurements taken from ACE-MAESTRO's UV- and visible-range spectrometers, and a study of ozone trends as observed by ACE-MAESTRO

Victoria Rose Spada

Winter 2021

Abstract

The ACE-MAESTRO (Atmospheric Chemistry Experiment - Measurement of Aerosol Extinction in the Stratosphere and Troposphere Retrieved by Occultation) has been in orbit on the SCISAT satellite for 17 years. It comprises two independent diode-array spectrometers. This report discusses a study of measurements from ACE-MAESTRO's two spectrometers, from data versions 1.2 and 3.13.

The first objective of this study was to determine where there are differences between the measurements taken by ACE-MAESTRO in the UV and VIS spectral regions. This was done by comparing simultaneous ozone measurements from ACE-MAESTRO's two spectrometers. Comparisons were performed for the complete data sets and year-by-year to investigate yearly patterns. This was done for measurements from version 1.2 (from the UV and VIS spectrometers) and 3.13 (from the VIS spectrometer only).

The second objective of this study was to examine ozone trends as observed by ACE-MAESTRO. To model the temporal development of atmospheric ozone, version 1.2 and/or 3.13 ozone measurements from the two spectrometers, two methods were used. For the first method, a deseasonalisation was done by subtracting the average monthly ozone quantities, fitting a straight line to the deseasonalised monthly values, and adding back the seasonal averages. For the second method, a multilinear trend model consisting of a linear term and several harmonics was used. To begin, the temporal development of ozone was modelled as a straight line, and then sinusoidal terms with various periods (28, 12, 9, 8, 6, 4, and 3 months) were introduced to fit the measured data set.

1 Introduction: About ACE-MAESTRO

1.1 Purpose

The ACE-MAESTRO (Atmospheric Chemistry Experiment - Measurement of Aerosol Extinction in the Stratosphere and Troposphere Retrieved by Occultation) has been in orbit on the SCISAT satellite for 17 years since its launch in August 2003. The goal of the ACE mission, associated with the SCISAT satellite, is to study the composition of the Earth's atmosphere, with a particular emphasis on stratospheric ozone distribution and related trace gases in the Arctic [1].

ACE-MAESTRO has two independent diode-array spectrometers: one measures ultraviolet (UV) and visible (VIS) spectra, and the other measures near-infrared (NIR) and VIS spectra.

ACE-MAESTRO and ACE-FTS (Atmospheric Chemistry Experiment - Fourier Transform Spectrometer) are the two instruments on the SCISAT satellite that contribute to the ACE mission. The main objectives for the ACE mission, as described by Bernath et al. [2], are:

1. to better evaluate and quantify the chemical and dynamical processes impacting the distribution of ozone in the stratosphere and upper troposphere;

2. to examine the relationship linking atmospheric chemistry and global climate change;

3. to study how burning biomass affects the free troposphere; and

4. to establish/verify aerosol and cloud properties, to lower their uncertainties for the quantification of their effects on the global energy balance [2].

Studying and tracking the atmosphere's ozone chemistry is the highest priority for the ACE mission. Studying the ozone budget is of particular importance because of changes in anthropogenic activity that impacted atmospheric ozone, which led to the Montreal Protocol in 1987. An increase in anthropogenic emission of CFCs (chlorofluorocarbons) led to an increase in ultraviolet (UV) radiation reaching the Earth's surface, and may also affect climate [2].

To understand the global ozone budget, extensive measurements of several species (such as O3, H2O, NO, NO2, N2O5, HNO3, HNO4, HCl, ClNO3, and ClO) are needed, along with measurements of aerosol extinction in the UV, visible (VIS), and near-infrared (NIR), and range. These measurements are necessary to determine the composition, size, and density of aerosols and polar stratospheric clouds, on which ozone molecules are vulnerable to being destroyed [1].

Though ACE-FTS can measure aerosol extinction (in the mid-IR spectral region) and up to 33 trace gases [2], the capabilities of the ACE mission were greatly enhanced by the addition of ACE-MAESTRO, as its UV-VIS-NIR spectrometers extended the wavelength range of the ACE measurements, particularly for aerosol extinction measurements, and provided some scientific and mission redundancy [1]. The main scientific contributions to the ACE mission associated with adding ACE-MAESTRO include the collection of aerosol extinction data in the 400–1010 nm wavelength range and the measurement of NO2 and ozone profiles with higher vertical resolution and precision than ACE-FTS. Measurements from ACE-FTS have a vertical resolution of ∼4 km, while measurements from ACE-MAESTRO have a vertical resolution of ∼1–2 km [1]. The addition of ACE-MAESTRO also improved the traceability of ozone measurements to other UV-VIS-NIR satellite measurements [1].

ACE-MAESTRO solar occultation spectral measurements in the UV-VIS-NIR are particularly useful because in this region there are major absorption features due to ozone, nitrogen dioxide, water, and molecular oxygen, in addition to scattering by molecules and aerosols. ACE-MAESTRO also has a secondary backscattering measurement mode for observing sunlight scattered back into space from the atmosphere, enabling the global mapping of ozone and NO2 total column amounts [1].

With each orbit, ACE-MAESTRO takes up to 2 occultations (one sunrise and one sunset). ACE-MAESTRO completes around 15 orbits per day. Figure 1 shows a butterfly plot of the latitudinal distribution of ACE-MAESTRO's measurements and a map showing the exact locations of measurements from ACE-MAESTRO over one year (2009).

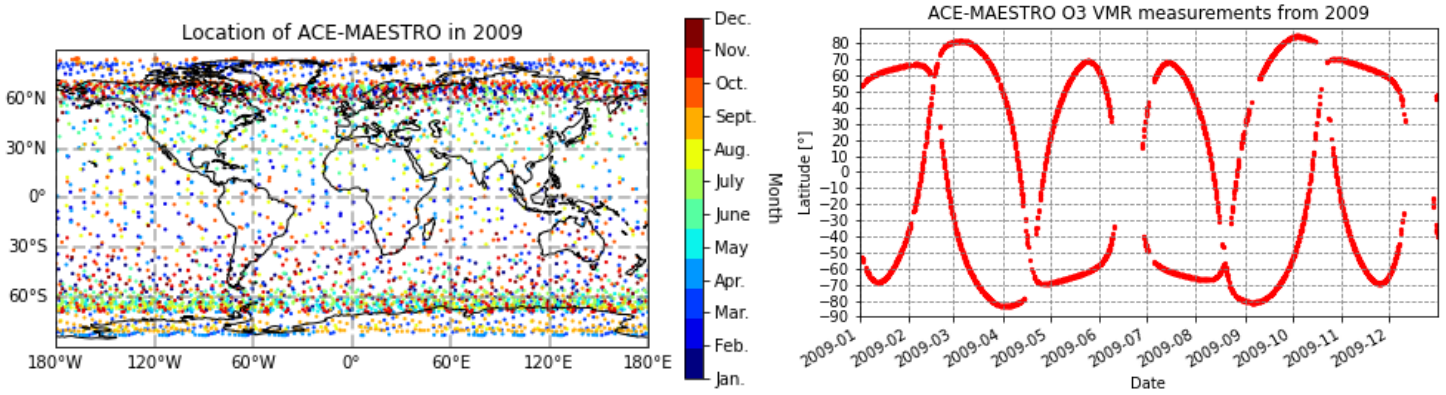

(a) (b)

Figure 1: A world map showing the exact locations of measurements from ACE-MAESTRO in 2009, and a butterfly plot showing the latitudinal distribution of measurements for that year.

1.2 Functions

ACE-MAESTRO has two independent diode-array spectrometers, one that measures spectra from 285 to 565 nm, with a 1.5 nm resolution (this is referred to as the UV spectrometer), and one that measures in the range from 515 to 1015 nm, with a 2 nm resolution (referred to as the VIS spectrometer) [1]. Measurements of ozone are collected by solar occultation.

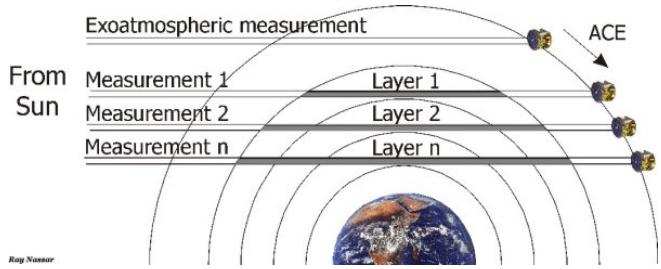

Figure 2: Diagram of how measurements are taken by solar occultation [3].

Solar occultation is a technique in which the transmission of sunlight through the Earth's atmosphere is measured relative to exoatmospheric measurements. As shown in Figure 2, this is done by taking a series measurements at different tangent heights. From each of the atmospheric measurements a slant column is obtained, and these can be combined to find vertical column density [3].

Slant column densities express the amount of a particular molecule (ie, ozone) along the path that light from the Sun to Earth, reflected from Earth's surface, and reaching the instrument performing the measurement. The vertical column density quantifies the amount of a molecule directly above a point on Earth's surface; it is generally more useful for analysis than the slant column density [4].

A sunrise or sunset occultation measurement sequence usually takes 1-3 minutes and consists of approximately 60 spectra taken at tangent altitudes from 0-100 km, and 20 spectra collected from the thermosphere for calculation of a Sun reference spectrum. Most measurements do not reach below 5–10 km because of clouds. A series of 80 spectra are collected when the Sun is below the horizon (before sunrise or after sunset), to use in the calculation of detector dark current. ACE-MAESTRO can also take backscatter measurements, but these are not used in this study [1].

1.3 Data Versions

Measurements from ACE-MAESTRO have been processed in several versions, the most recent being version 3.13. In this report, versions 1.2 and 3.13 are studied.

For processing data with the version 1.2 algorithm, the raw data from ACE-MAESTRO (Level 0 data) is first calibrated in wavelength and corrected for pixel integration times, dark current, stray light, and other parameters. This data (now at Level 1) is then used to obtain slant column densities and vertical profiles (Level 2 data) [1].

In general, a new data version is motivated by any number of the following factors:

1. "major forward model and/or retrieval algorithm changes;
2. input data changes such as version changes of the input ACE-FTS retrieved pressure and temperature (p,T) profile data;
3. changes of the tuning instrument parameters" [5].

For example, versions 1.1 and 1.2 were based on uniform version 2.2 of the ACE-FTS (p,T) profile data, but version 1.2 uses a different set of instrument parameters in time shift, UV spectrometer angle shift, and the VIS spectrometer angle shift [5]. Volume mixing ratios of nitrogen dioxide and ozone, and UV and VISIBLE optical depth are the routine products for this version. For each spectrometer (UV and VIS), both nitrogen dioxide and ozone profiles are available in two forms:

1. retrieved at the measurement tangent altitudes, and
2. interpolated at the regular tangent height grid from profile (1.) [5].

For version 1.2, measurements of type (2.) in the above list were used in this study. These version 1.2 measurement files include the ozone volume mixing ratios (ppv) and their fractional errors on a 0.5 altitude grid from 0-100 km. The retrieved measurements are given, and if no measurement was retrieved for a specific altitude, an a-priori measure of the ozone volume mixing ratio is given.

From studying versions 3.12 and 3.12.1, it was determined that two different scaling factors had to be used for the sunset and sunrise measurements [6]. Additionally, in versions 3.12 and 3.12.1, the same scaling factor is used

for each of the three data products: nitrogen dioxide profiles from the UV spectrometer and ozone profiles from the UV and VIS spectrometers. When version 3.13 was being developed, the scaling factor was chosen to attain the best data quality for ozone measurements from the VIS spectrometer, disregarding the UV spectrometer data quality [6]. This choice is largely a result of the fact that the UV spectrometer currently senses a small range of wavelengths and has significantly deteriorated since its launch in 2003. In general, measurements from October 2010 onwards are considered less useful and reliable. In contrast, the VIS spectrometer has behaved normally since its launch [6].

For this study, version 1.2 measurements from the UV and VIS spectrometers and version 3.13 measurements from the VIS spectrometer are used to compare the two spectrometers on ACE-MAESTRO. The available data from versions 1.2 and 3.13 span 2004-2011 and 2004-2020, respectively.

2 Methods

2.1 Comparison methods

Measurements taken from the same occultation were located using occultation IDs. For these comparisons, only measurements that were retrieved were included; a-priori measurements were not used. Measurements from version 3.13 were interpolated onto the version 1.2 grid (0-100 km, 0.5 km resolution) for these comparisons.

To compare the measurements, a linear regression was performed for each year of data that was taken. For each year, the measurements were categorized by altitude and scattered on a correlation plot. The measurements were examined over different altitude ranges: from 0-20 km, 20-60 km, and 60-100 km. The measurements were categorized by altitude because the general patterns of mean relative differences varied significantly by altitude. Two methods of regression were used: Ordinary Least Squares (OLS) and Reduced Major Axis (RMA) regression. These two methods of regression were used in a validation study of ACE and OSIRIS (Optical Spectrograph and Infra-Red Imager System) measurements [7]; since the RMA solution is symmetrical, the variables are not labelled as dependent and independent, which is more appropriate for these comparisons [7]. Errors of the measurements were not included in these regressions.

For N measurements, the mean absolute difference between two quantities x and y (here, two measurements of ozone from different spectrometers and/or data versions) is given as:

$$\Delta_{abs} = \frac{1}{N}\sum_{i=1}^{N}(x_i - y_i) \tag{1}$$

and the mean relative difference of the two quantities is written as:

$$\Delta_{rel} = \frac{1}{N}\sum_{i=1}^{N}\frac{(x_i - y_i)}{(x_i + y_i)/2}\cdot 100\% \tag{2}$$

These two metrics quantify systemic error between the measurement sets. The root-mean-square deviation (RMSD) of two measurement sets is shown in equation 3.

$$RMSD = \sqrt{\frac{1}{N}\sum_{i=1}^{N}(x_i - y_i)} \tag{3}$$

$$R = \frac{\sum_i (x_i - \bar{x})(y_i - \bar{y})}{\sqrt{(\sum_i (x_i - \bar{x})^2 \sum_i (y_i - \bar{y})^2)}} \tag{4}$$

The Pearson coefficient (equation 4), root-mean-square deviation (equation 3), and mean absolute and relative differences (equations 1 and 2) were calculated for simultaneous measurements, including each retrieved point on the version 1.2 altitude grid from each measurement. These metrics are often used in comparison and validation studies for satellite measurements [7, 8, 9]. The mean absolute and relative difference profiles for each comparison were also calculated for each comparison pair, for each year, and cumulatively from 2004-2011.

2.2 Modelling Atmospheric Ozone in Space and Time

The objective of this section was to consider different ways of modelling Earth's atmospheric ozone in space and time, as seen by ACE-MAESTRO. First, time series of measurements of ozone from altitudes 0-100 km from versions 1.2 (UV and VIS) and 3.13 (VIS) were constructed from monthly averages of ozone measurements. The measurements were kept on the altitude grid that they came on.

Measurements were further categorized by latitude, with latitudinal resolutions of 5° and 30°. Using a resolution of 30° allowed for more measurements to be included for each time series and results in a more robust fit. In the following sections, the two methods implemented for modelling the monthly ozone averages for each (altitude, latitude) point are introduced.

2.2.1 Deseasonalisation method

The first, simpler model involves finding the average ozone amount for each month (January-December) and subtracting the average amount from each month to deseasonalise the data set. Then, a straight line $\hat{\boldsymbol{y}} = a + b\boldsymbol{x}$ was fit through the deseasonalised data using a parametric trend model (see Appendix A). The monthly averages were then added the straight line to yield the finished model. To have a number of data points for each month of the year, a 30° latitude grid was used.

2.2.2 Multilinear parametric trend model

A multilinear parametric trend model was used to model each of the three ozone data sets over altitudes ranging from 0-100 km, for all latitudes. The model includes a constant and a linear term, annual and semi-annual oscillation terms, in addition to several harmonic terms, and was taken from von Clarmann et al [10] (see Appendix A).

$$\hat{y} = a + bx + \sum_i \left(c_i sin(\frac{2\pi x}{l_i}) + d_i cos(\frac{2\pi x}{l_i}) \right) \tag{5}$$

The parameters a and b are associated with the linear trend, and the parameters c_i and d_i are associated with each oscillation of length l_i months included in the model. Oscillaing terms of periods 28, 12, 9, 8, 6, 4, and 3 months were included. Von Clarmann et al. recommends using the full covariance matrix for this trend model to eliminate bias [10], but the matrix is not available for the data sets being used, so the covariances were taken to be zero and the errors of the measurements were used as the variances. This approach is similar to the approach taken in Eckert et al. [11].

2.2.3 Determining the number of years required to detect a linear trend

It is important to ensure that a data set used for a model covers a long enough time span to accurately describe the trend. Recalling that the data available from versions 1.2 and 3.13 span 2004-2011 and 2004-2020 respectively, the two data sets may not accurately detect the same linear trends.

Weatherhead et al. provides an outline for determining the minimum number of years of data n^* needed to accurately determine a linear trend ω_0, using the auto-correlation ϕ and monthly variation of the data sets σ_N [12]:

$$n^* = \left[\frac{3.3\sigma_N}{|\omega_0|} \sqrt{\frac{(1+\phi)}{(1-\phi)}} \right]^{2/3} \tag{6}$$

The value of n^* found by using equation (6) assumes that the model is linear and that the values of ϕ and σ_N are known. The values of ϕ and σ_N are not known for the ACE-MAESTRO version 1.2 and 3.13 data sets, so these values had to be estimated. The estimated values of ϕ and σ_N ($\hat{\phi}$ and $\hat{\sigma}_N$) can be plugged into equation (6). This makes the value of equation (6), n^*, an estimate as well ($\hat{n}^*$).

Weatherhead et al. states that in practice, generally only a few years of data are needed to attain a fairly good estimate of σ_N, so it is usually acceptable to ignore the uncertainty in $\hat{\sigma}_N$ (i.e., one can approximate $\hat{\sigma}_N = \sigma_N$) [12]. In general, more time (ie, a longer data set) is needed to adequately estimate ϕ [12]. For each model in this study, the entire data sets were used to estimate σ_N and ϕ.

Since n^* was estimated as $\hat{n}^*$, it's uncertainty required quantification. Weatherhead et al. provides the following equation for the 95% confidence interval for n^* when $\hat{\phi}$ is the least-squares estimate of ϕ, using M months of data [12]:

$$\left(n^* e^{-B}, n^* e^{B}\right) \tag{7}$$

where

$$B = \frac{4}{3\sqrt{M}} \sqrt{\frac{1+\hat{\phi}}{1-\hat{\phi}}} \tag{8}$$

Note that $\hat{\phi}$ is the estimate of ϕ calculated from the data set.

Equation (6) was also inverted to solve for the minimum drift that could be calculated for the version 1.2 and 3.13 data sets, which are 8 and 16 years long respectively:

$$|\omega_0|_{min} = \left(\frac{1}{n^*}\right)^{3/2} \left[3.3\sigma_N \sqrt{\frac{(1+\phi)}{(1-\phi)}}\right] \tag{9}$$

For each point on the altitude/latitude grid, after the linear drift parameter was determined using either of the two methods outlined above, it was checked whether the drift was greater than or equal to the drift found from equation (9); points that did not meet this criteria were filtered out. It was also checked if the linear drift for each point was greater than its uncertainty. These points were filtered out as well, but this creates a strong bias against points where the drift was actually very small, since a very small uncertainty would be required.

3 Results

3.1 Comparisons between UV and VIS spectrum measurements

The ACE-MAESTRO UV 1.2, VIS 1.2, and VIS 3.13 data sets were compared, and the results are discussed in this section.

3.1.1 Point Comparisons

Comparing the three data sets point-by-point, scatter plots were made and linear regressions were performed. For each coincident occultation, there is a maximum of 201 measurements of ozone from each data version, as the data comes from 0-100 km on a 0.5 km grid (the grid is finer for version 3.13, but for comparisons, version 3.13 measurements were interpolated onto the version 1.2 0.5 km grid).

The coincident measurements were scattered, and to quantify their relationship, the quantities shown in Table 1 were computed for each pair. The comparisons were done year-by-year and also over the entire comparison period of 2004-2011. The relative differences for each year are shown in Appendix B. These results were aggregated to produce the results shown in Table 1.

Figure 4 shows the coincident measurements used in the pointwise comparisons, separated by altitude. None of the scatter plots qualitatively show a purely 1:1 relationship, aside from measurements ranging in the 20-40 km range, where for all comparisons there seems to be the best correlation. This region is where the ozone layer is, so the maximum of ozone is expected to exist in this region for each measurement. Since the amount of ozone reaches a peak in this altitude region, it makes sense that the relative difference would be lowest there. At other altitudes, the measurements visually appear completely uncorrelated. From around 0-10 km and 50-100 km, measurements of ozone from the VIS version 3.13 data set appear to plateau around 0.2^{-5} ppv, while the measurements from the version 1.2 data sets vary.

The OLS and RMA fits were all found to be quite poor for each of the comparisons. These regressions were performed for the yearly and cumulative data sets. The altitude ranges with poor correlation dominated the regressions, resulting in extremely steep lines for the comparisons including VIS version 3.13 measurements, with slopes on the order of 10 up to 100,000. The comparison between the version 1.2 data sets (UV 1.2 and VIS 1.2) yielded slopes much less than 1. An example of this is shown in Figure 5, which shows the linear regressions and Pearson coefficients for the 2009 comparisons.

	v.1.2 UV - v.1.2 VIS	v.3.13 VIS - v.1.2 UV	v.3.13 VIS - v.1.2 VIS
Number of Measurement Pairs	1736787	1650983	1651907
Mean Absolute Difference [ppv]	1.31e-4 ± 0.42e-5	-4.41e-5 ± 1.40e-5	-3.93e-5 ± 1.34e-5
Mean Relative Difference [%]	27.2 ± 3.5	-32.8 ± 7.8	-31.2 ± 8.5
RMSD [ppv]	1.73e-30.001725935	7.27e-3	4.3e-3

Figure 3: Table 1. Results of comparing measurements from the ACE-MAESTRO UV 1.2, VIS 1.2, and VIS 3.13 data sets, over a temporal range from 2004-2011.

3.1.2 Profile Comparisons

The measurements were compared as profiles for each data set. First, the average ozone profiles were calculated for each of the three data sets. All measurements from the comparison time period of 2004-2011 were included, but points that were not retrieved were excluded. The profiles are shown in Figure 6. A large portion of the atmospheric ozone is shown to be in the stratosphere, with a peak around 35 km for each version; this is the ozone layer. Measurements above outside of the 20-60 km are retrieved with a much lower frequency than the stratospheric altitudes. The two data sets from version 1.2 show a second peak above the ozone layer. These measurements often have a high uncertainty and are retrieved less often. These peaks were not expected to exist in the data sets and show that the measurements are generally less reliable in the troposphere and above the stratosphere.

To study the average differences between the ozone profiles, coincident occultation profiles were subtracted from each other, and these differences were averaged over each year to obtain the average absolute and relative difference profiles for each year as well as over the entire comparison period of 2004-2011. The yearly mean absolute and relative difference profiles for each pair are shown in Figures 7, 8, and 9.

Figure 7 shows the mean absolute and relative differences between the ACE-MAESTRO UV 1.2 and VIS 1.2 data sets. Note that the range of the differences on the x axis varies for each subfigure; this is why the differences as a function of altitude are split up into three subplots.

In Figure 7, from 0-20 km, the differences are generally negative, indicating that the measurements from the ACE-MAESTRO VIS 1.2 data set showed higher ozone amounts. In contrast, in the upper altitudes from around 60-100 km, the measurements from the UV 1.2 data set are generally larger, on the same order of magnitude as in the lower region. In the 0-20 km and 60-100 km regions, the magnitudes of the mean absolute differences are on the order of around 0.01 ppv and the magnitudes of the mean relative differences are on the order of around 200%. The measurements in the 20-60 km range show the lowest mean absolute and relative differences, which are on the order of around 10^{-6} ppv and 10%, respectively. This altitude range contains the ozone layer (ie, this area contains the most ozone), so it is anticipated that the mean relative differences would be lower here. The profiles appear to be scattered about the zero point.

Figure 8 shows the mean absolute and relative differences between the ACE-MAESTRO VIS 3.13 and UV 1.2 data sets. Notably, the curves for each year start at around 10 km, which indicates that no retrieved coincident measurements at altitudes below 10 km were found. In the altitude regions from 10-20 km and 60-100, the mean absolute and relative differences are generally negative, indicating that the measurements from the UV 1.2 data set are generally greater than the measurements from the VIS 3.13 data set. Similar to what was seen in Figure 7, Figure 8 shows that the comparisons in the altitude range from 20-60 km yielded the lowest mean absolute and relative differences. It generally looks like the differences are negative in this altitude range, with the exception of the years 2004 and 2010, which show positive mean absolute and relative differences. There is a large spike in the 2009 difference profiles in the 20-60 km region. The cause of this spike is not known, but it is probably the result of an outlier or some error in a retrieval from the VIS 3.13 data set (this spike is only seen in the comparisons including VIS 3.13 data). Figure 9 shows the mean absolute and relative differences between the ACE-MAESTRO VIS 3.13 and VIS 1.2 data sets. This figure looks very similar to the result of comparing the VIS 3.13 and UV 1.2 data set.

The results from Figures 7, 8, and 9 were aggregated into mean absolute and relative difference profiles over the entire time period of 2004-2011, and the result is shown in Figure 10. In the altitude range from 0-20 km, the differences including the VIS 3.13 data are generally smaller, but in the 60-100 km region the differences for

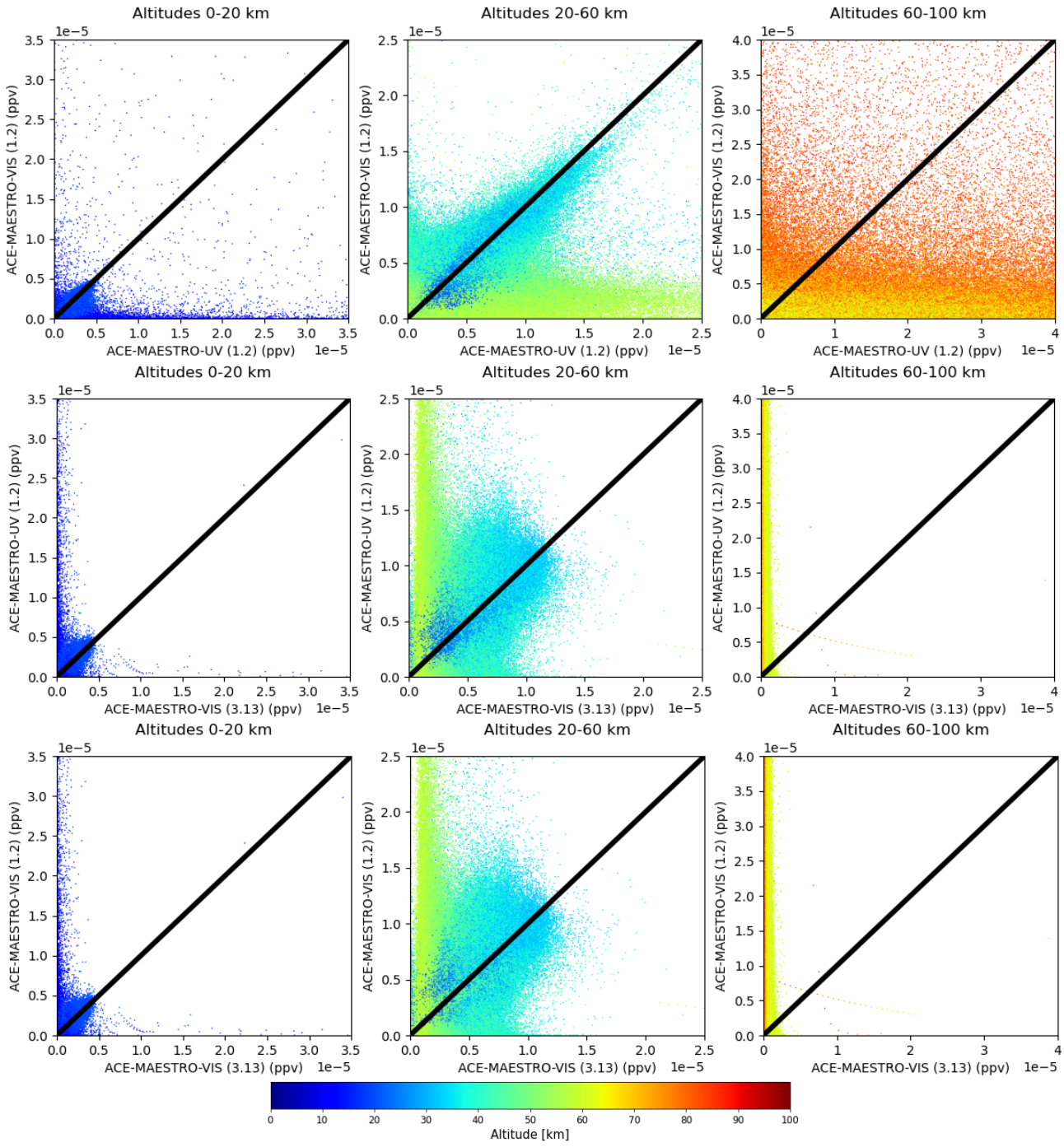

Figure 4: Scatter plots of ozone measurements from ACE-MAESTRO UV 1.2, VIS 1.2, and VIS 3.13. Measurements range from 2004-2011. The black lines show the ideal 1:1 correlation. The scatter plots also indicate the altitude of each ozone measurement.

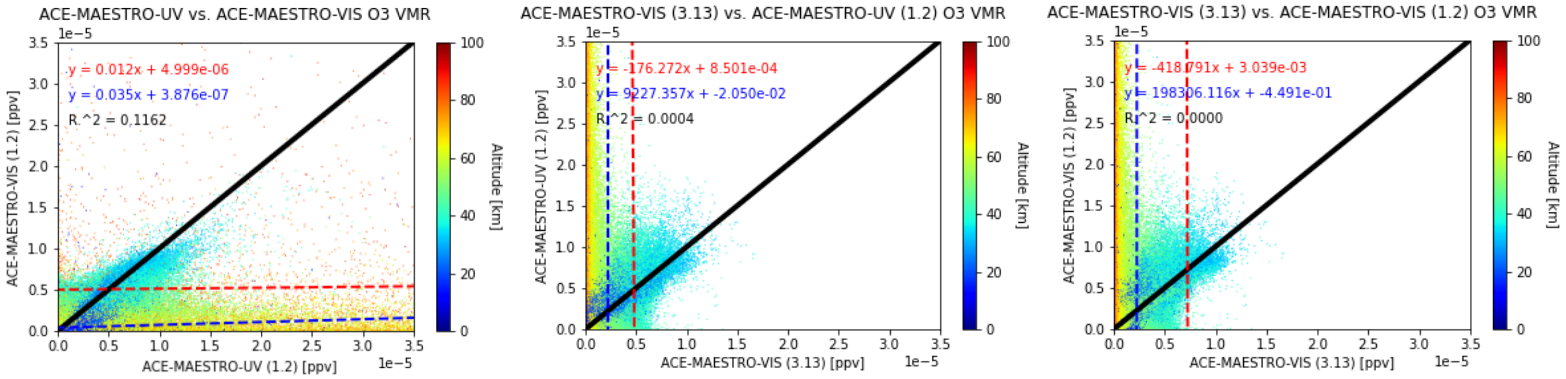

Figure 5: Example of scatter plots of ozone measurements from ACE-MAESTRO UV 1.2, VIS 1.2, and VIS 3.13 for the year 2009. The OLS fits are written in red and the RMA fits are written in blue. The Pearson coefficient is also indicated for each comparison.

these profiles are larger. From around 20-50 km, the mean relative differences are negative and lie in the range of around $[-20, -5]\%$.

The latitudinal variation in the differences was also examined. Figure 11 shows the mean relative difference profiles for each comparison on a 5° latitudinal grid. In general, the profiles look fairly similar across all latitudes. It is expected that measurements in the polar regions may vary due to the polar vortex, but this is not totally seen due to the data availability, and where data is available, the profile looks consistent with profiles corresponding to other latitudes. Figure 11 visualises how in the 0-15 km and above around 60 km, the magnitudes of the differences are at their greatest. This is due to the lower retrieval rates at these altitudes, and also because of clouds in the troposphere. Across the three comparisons it appears that the peak differences in the troposphere/tropopause in the polar regions are located closer to Earth's surface than it is at the equator. This may be due to clouds forming at higher altitudes near the equator, lowering the number of retrievals and increasing the uncertainty of these measurements [13, 15, 14].

3.2 Modelling Atmospheric Ozone

The three ACE-MAESTRO data sets (UV 1.2, VIS 1.2, and VIS 3.13) were modelled in space and time using the two methods described in sections 3.2.1 and 3.2.2. Below is a discussion of the results for each model.

3.2.1 Method 1: Deseasonalisation

Figures 12, 13, and 14 show the main results of implementing the deseasonalisation method to model the UV 1.2, VIS 1.2, and VIS 3.13 ACE-MAESTRO ozone data sets. These results are shown on a 30° latitudinal grid. The results are shown for modelling all (altitude, latitude) points as well as after filtering out the points where there was not enough data to accurately model the drift (found using the method described in section 3.2.3), and after further filtering out points where the drifts were less than their uncertainty.

Figure 12(a) shows the results for the linear drifts calculated for the UV 1.2 data set. At the highest altitudes and at altitudes around 10-15 km, the drifts are particularly high in magnitude; this is likely a result of lower frequency of retrievals and higher uncertainty of measurements at these altitudes. Some of these values go up to the order of $10^{-3} ppv/decade$, which does not seem reliable.

The polar regions (note that 'polar regions' is referring to the points in the 60°-90° North and South ranges on these plots) show drifts of the highest magnitude, with strong positive drifts above around 35 km, and strong negative drifts below 35 km. Figure 12(b) shows that the uncertainty of the drifts at high altitudes at the poles are particularly high, and most of them are filtered out in Figure 12(c). Most of the drifts shown in Figure 12(a) are too small to be accurately estimated by the given data set, as shown in Figure 12(c). 12(d) shows the points from Figure 12(c) further filtered to exclude points where the drift is less than its uncertainty.

Figure 13(a) shows the results for modelling the VIS 1.2 data set with the deseasonalisation method. The spread of the linear drifts shown in Figure 13(a) looks similar to the spread shown in Figure 12(a), except here the drifts at high altitudes in the non-polar latitudes have a lower magnitude. Many of the points in the polar

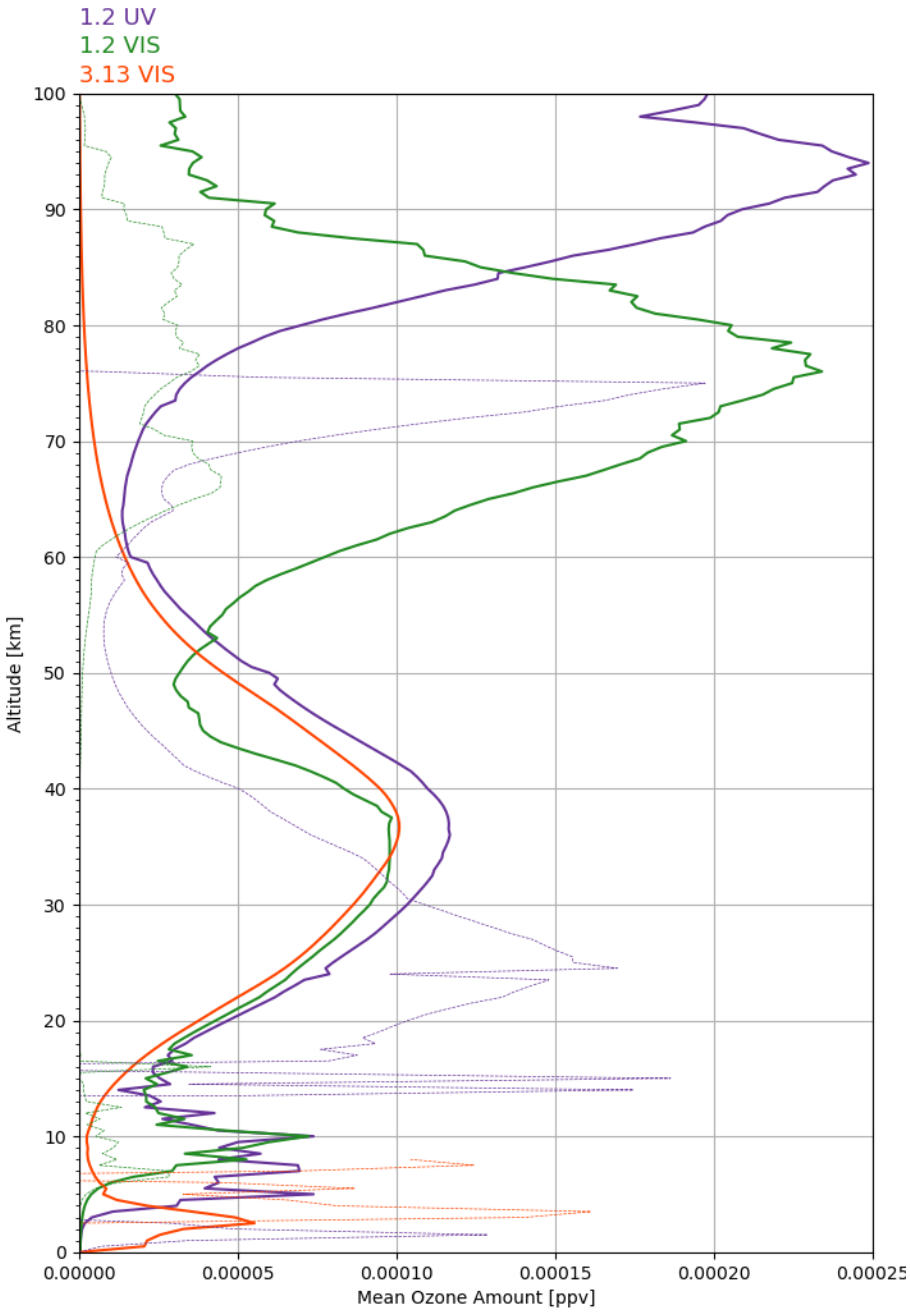

Figure 6: Average profiles from the UV and VIS spectrometers versions 1.2 and 3.13, from 2004-2011. Only retrieved measurements were included.

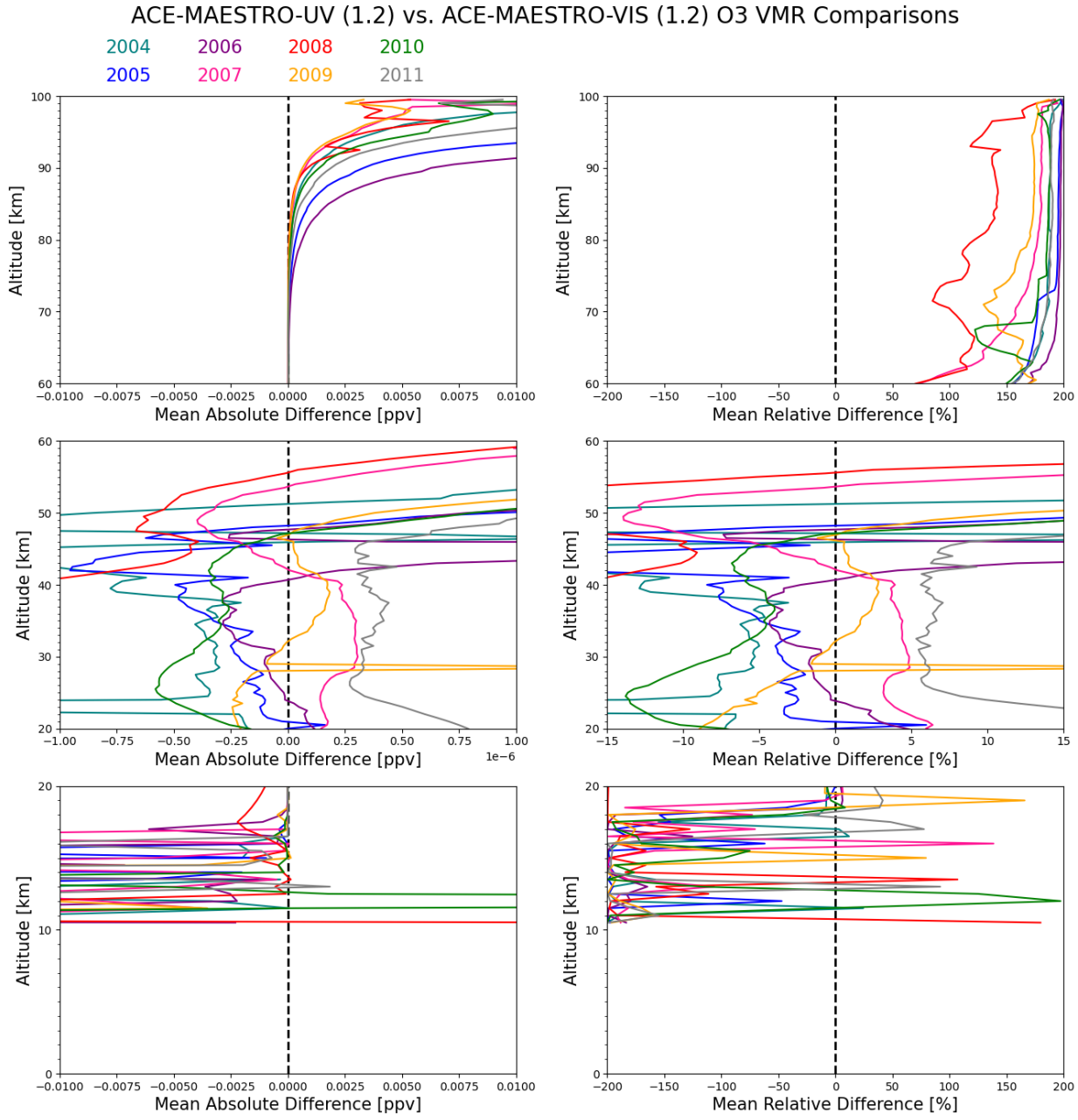

Figure 7: ACE-MAESTRO-UV (1.2) vs. ACE-MAESTRO-VIS (1.2) ozone mean absolute and relative differences as a function of altitude. Only retrieved measurements were included.

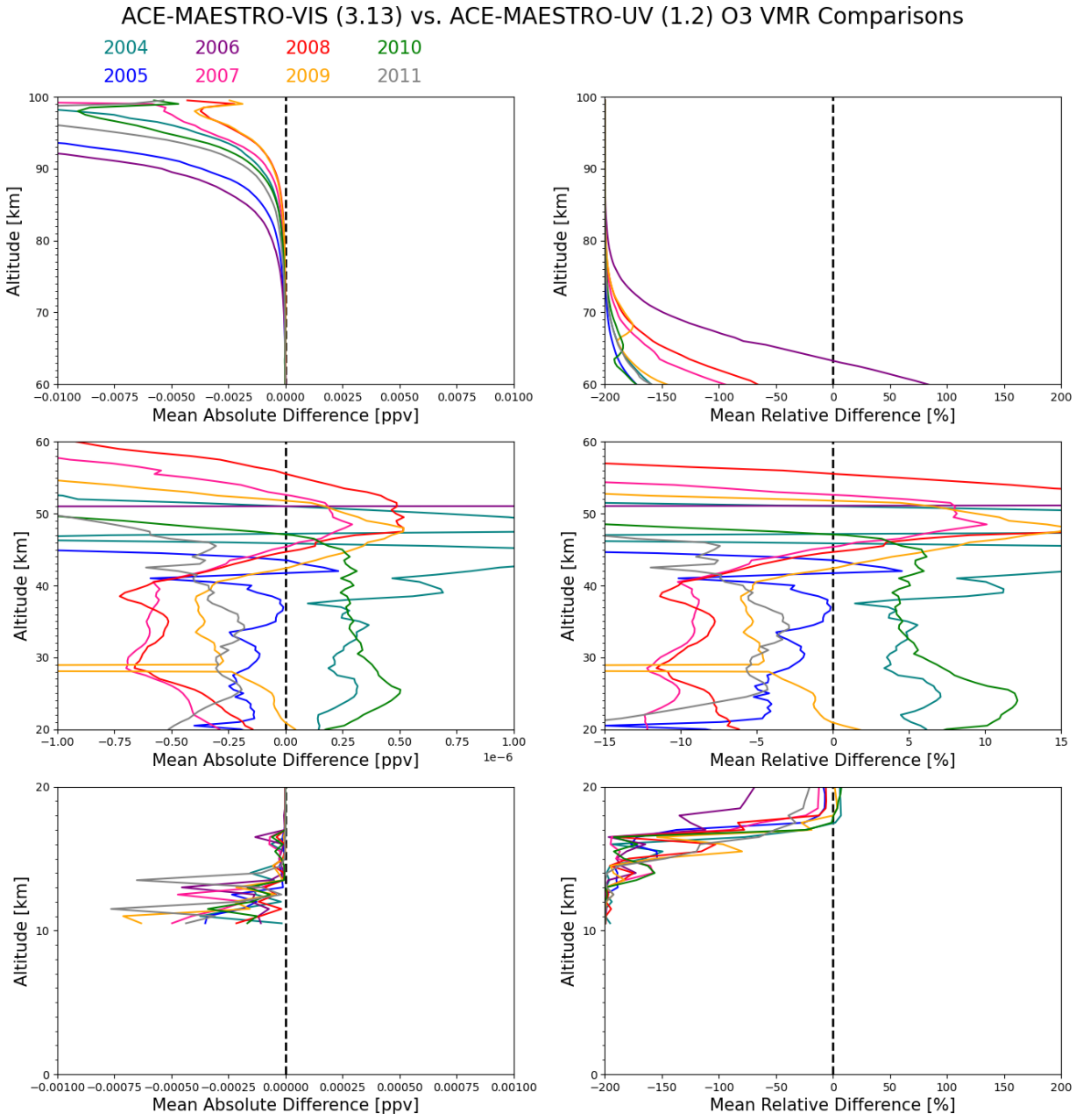

Figure 8: ACE-MAESTRO-VIS (3.13) vs. ACE-MAESTRO-UV (1.2) ozone mean absolute and relative differences as a function of altitude. Only retrieved measurements were included.

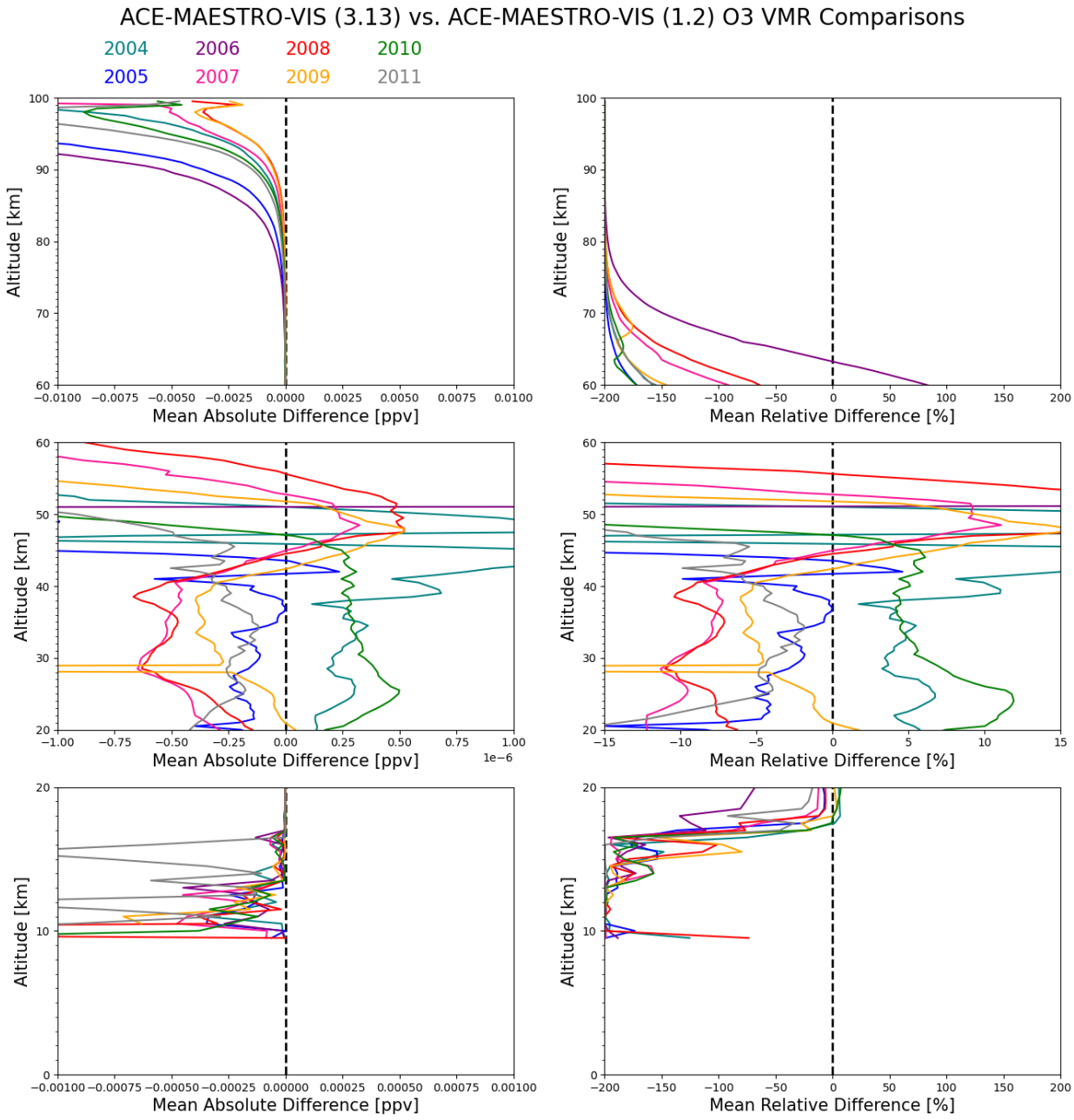

Figure 9: ACE-MAESTRO-VIS (3.13) vs. ACE-MAESTRO-VIS (1.2) ozone mean absolute and relative differences as a function of altitude. Only retrieved measurements were included.

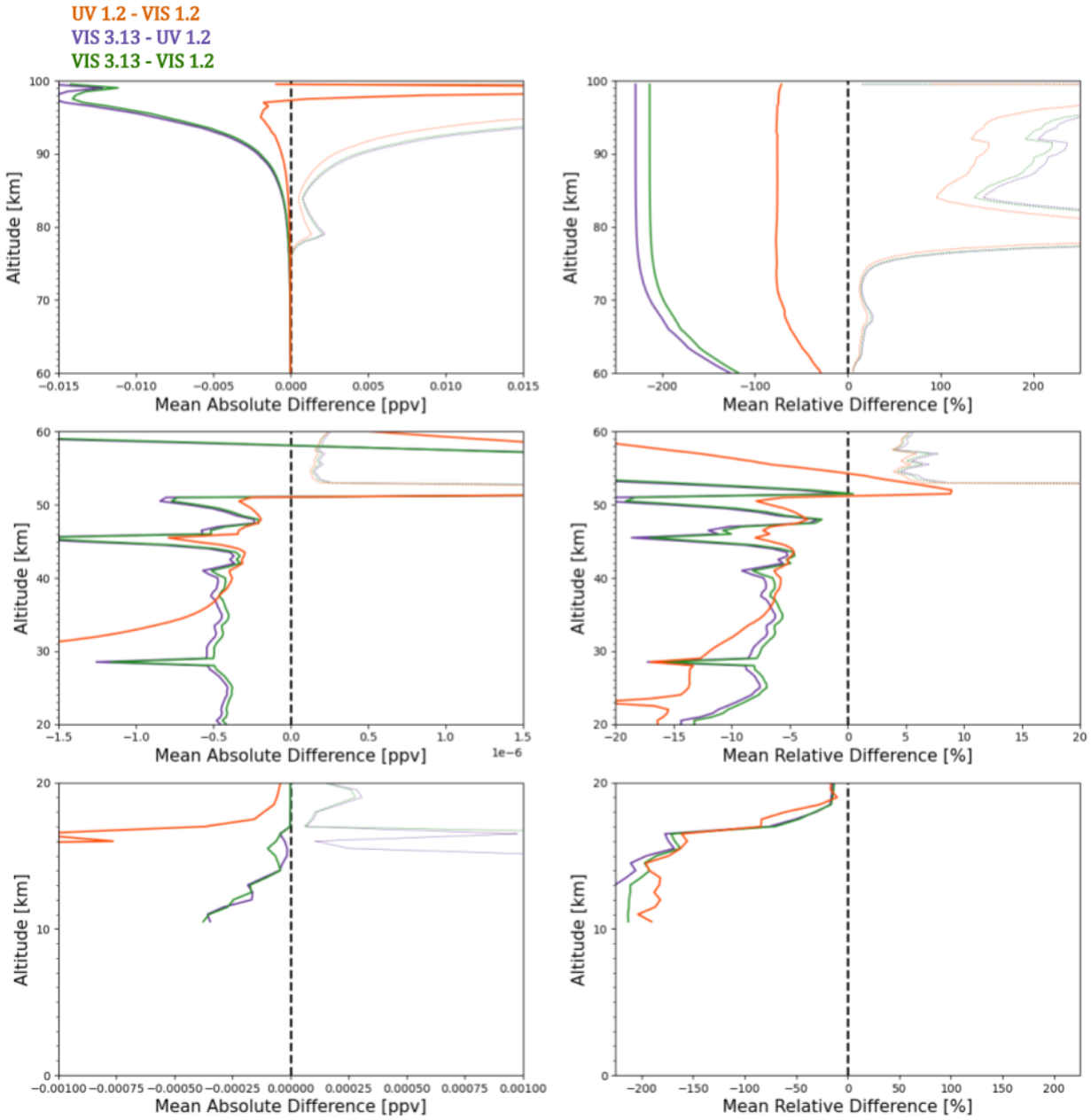

Figure 10: ACE-MAESTRO-VIS (1.2 and 3.13) vs. ACE-MAESTRO-VIS (1.2) ozone mean absolute and relative differences as a function of altitude, including measurements from 2004-2011. Only retrieved measurements were included. The errors of these profiles are shown as the thinner, dotted lines.

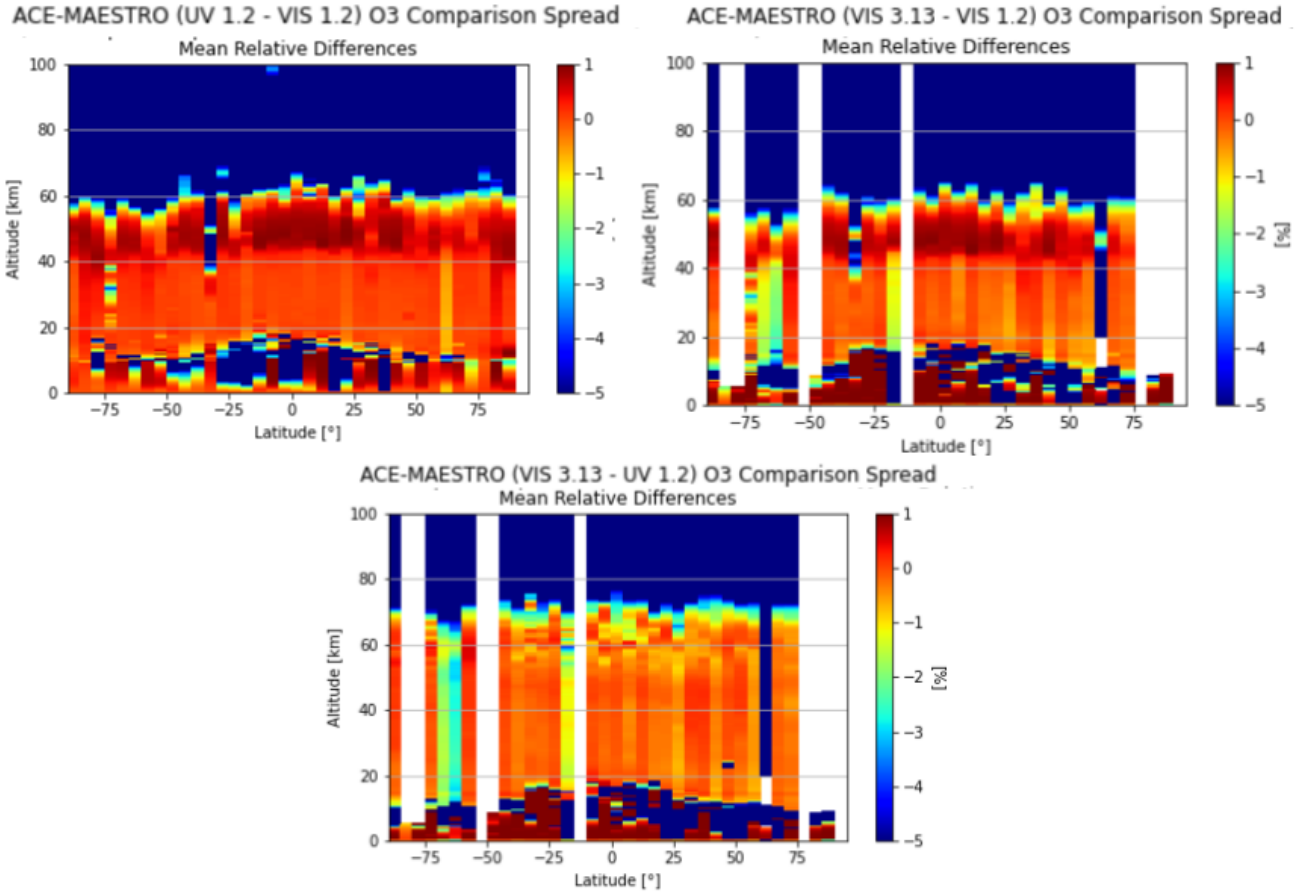

Figure 11: Plots of the mean absolute relative differences for each of the three comparisons, as functions of latitude and altitude.

region were not filtered out, and hardly any points were kept outside the polar region. These points show a very strong drift, on the order of around $10^{-4} ppv/decade$, which is much greater than the order of $ppmv$, so it is surprising that these points were not filtered out. This may be a result of the fact that the autocorrelation and variance of the measurements was estimated for this method. This result should be further investigated.

Figure 14(a) shows the results for the VIS 3.13 data set. The general spread of the drifts looks different for this data set than what was observed for the version 1.2 data sets. As with the models produced with this method using version 1.2 data, the drift in ozone was found to be generally positive at the North Pole, while at the South Pole, the drifts are negative below around 48 km. Above around 48 km, the drifts globally are generally positive or small and negative. The strong difference in the drifts between measurements below 48 km and those above 48 km may be a result of the measurement quality and infrequency of measurements above this altitude. It has already been discussed that measurements are retrieved less frequently in this region. The reason this difference is more notable for this data set is likely because this data set it twice as long as the data sets associated with version 1.2. Since this data set is much longer, the uncertainties of the drifts shown in Figure 14(b) are less than those observed for the models of the other two data sets. Additionally, since this set is longer, there are more points that passed the filtering before Figure 14(c) and (d).

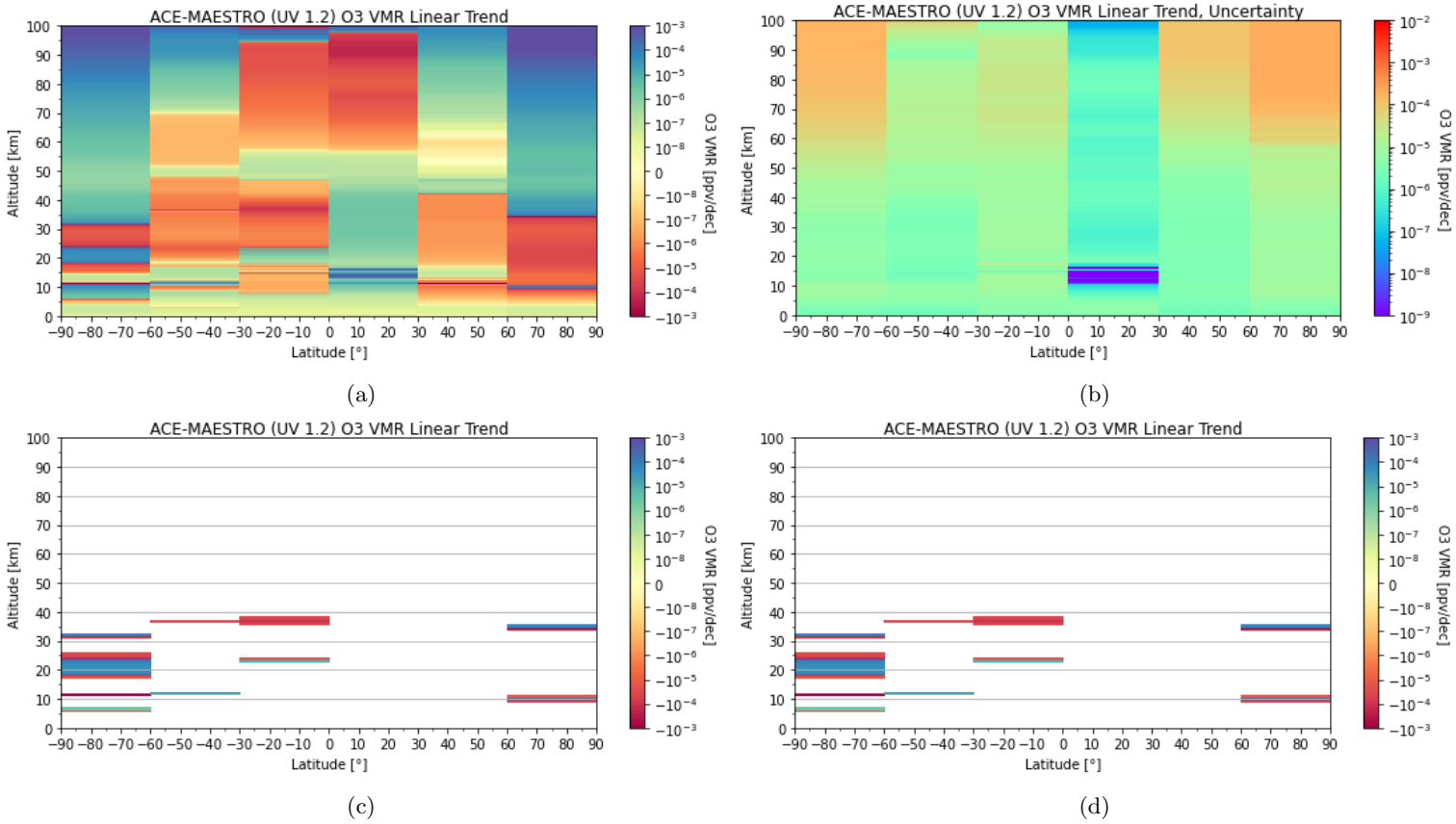

Figure 12: Results of modelling ACE-MAESTRO-UV 1.2 data from 2004-2011 using the deseasonalisation method. (a) shows the linear drift in ozone in [ppv/dec]; the uncertainties associated with (a) are shown in (b). (c) shows the result of filtering out points where $|\omega_0|_{min} \leq |\hat{\omega_0}|$ (where the estimated drift was found to be less than the minimum drift that could be estimated by the data set, found from equation 9). (d) shows the result of further filtering (c) to exclude points where the uncertainty of the drift was greater than the drift itself.

3.2.2 Method 2: Multilinear Parametric Trend

Figures 15, 16, and 17 show the main results of implementing the multilinear parametric trend model for the UV 1.2, VIS 1.2, and VIS 3.13 ACE-MAESTRO ozone data sets. These results are shown on a 30° latitudinal grid. The results of using the same model for the same data sets on a 5° latitudinal grid are shown in Appendix

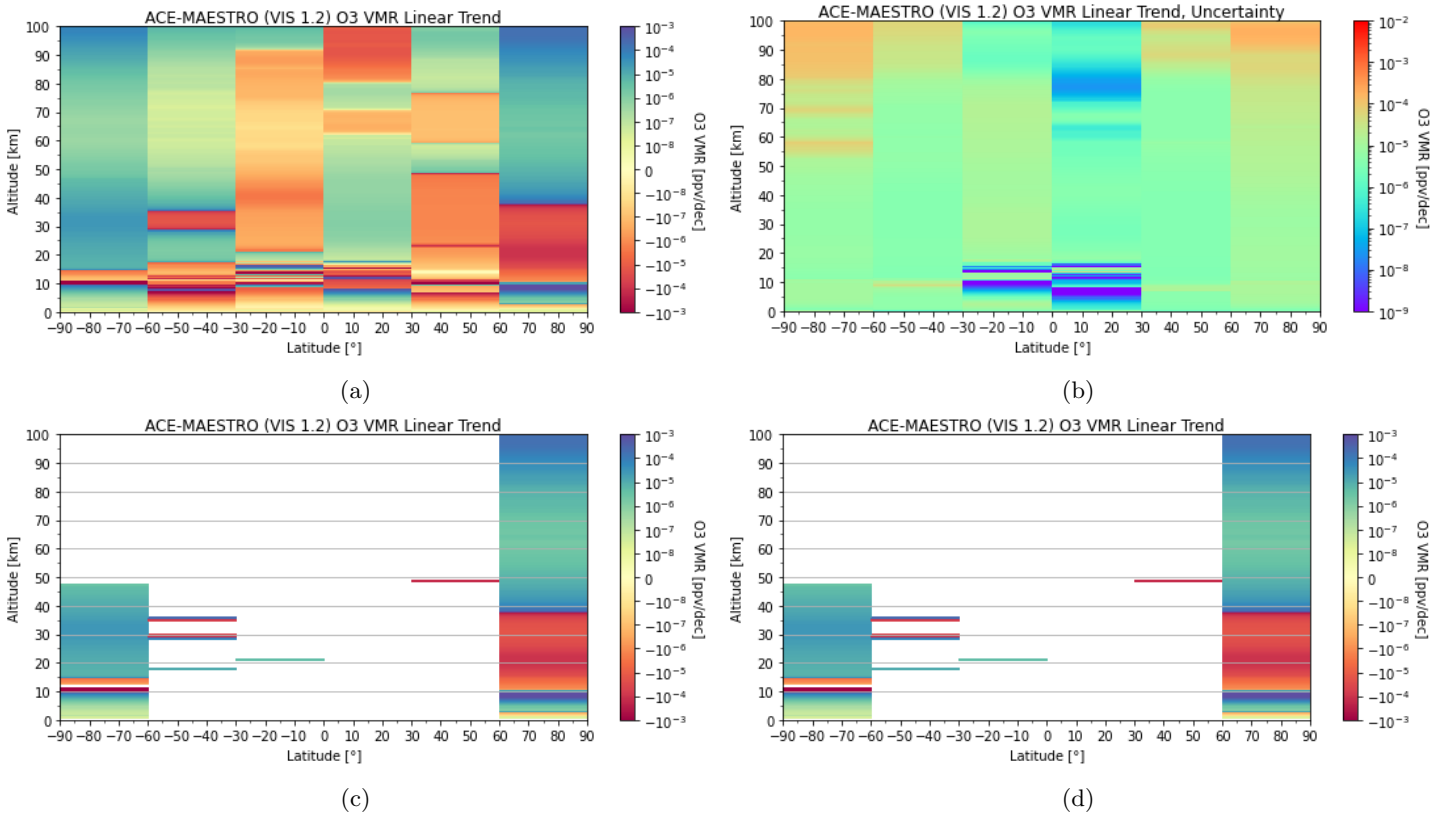

(a) (b)

(c) (d)

Figure 13: Same as Figure 12, but for ACE-MAESTRO-VIS 1.2 measurements from 2004-2011.

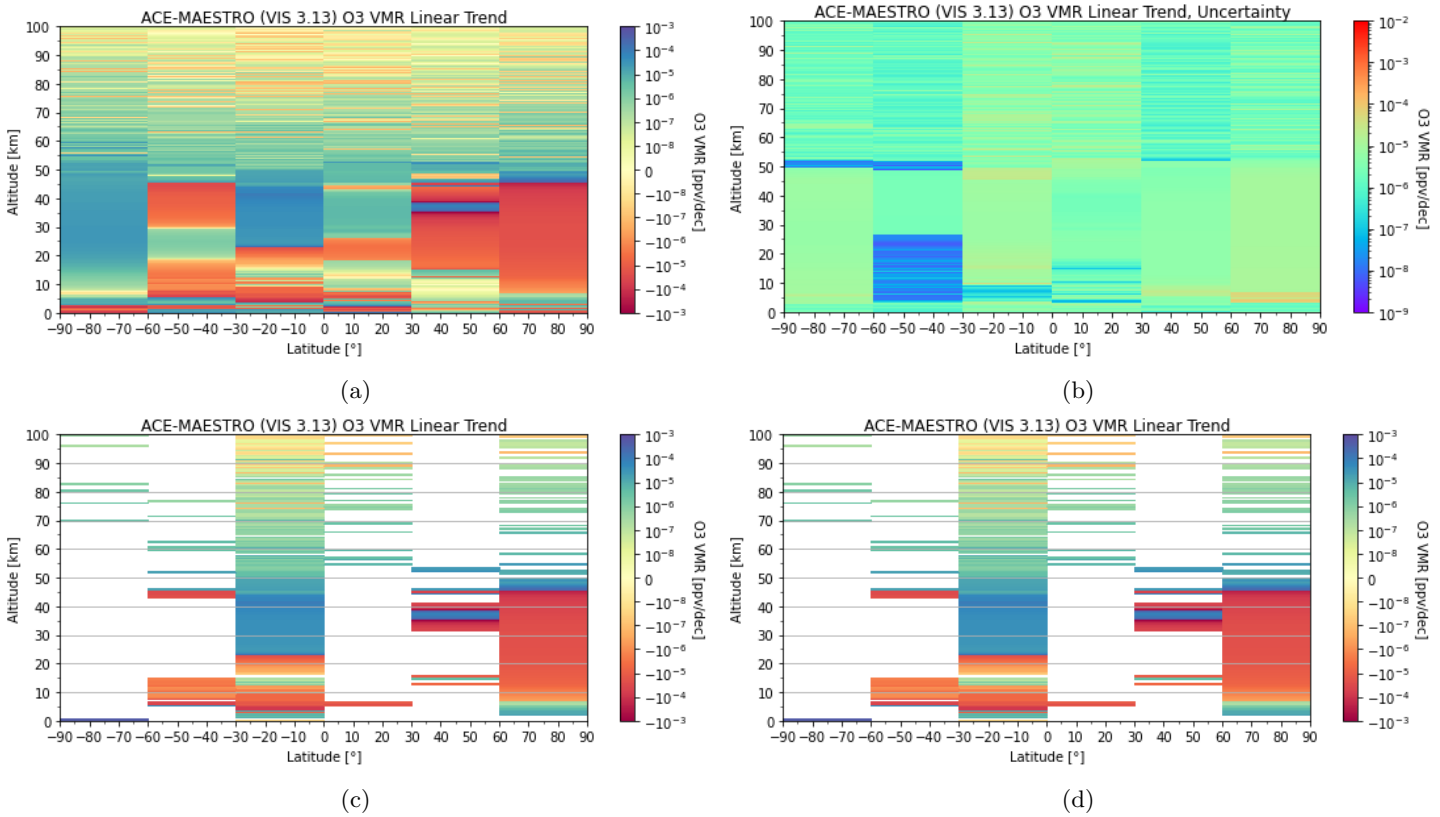

(a) (b)

(c) (d)

Figure 14: Same as Figure 12, but for ACE-MAESTRO-VIS 3.13 measurements from 2004-2020.

B (Figures 23, 24, and 25).

Figure 15(a) shows the results for the UV 1.2 data set. Notably, when this data set was modelled using the deseasonalisation method, the drifts in ozone at the northernmost latitudes were positive, but here they are mostly negative. The drifts generally appear to have higher magnitudes here than what was observed when modelling the data using the deseasonalisation method. At the highest altitudes and around 10-15 km, the drifts are particularly high in magnitude; this is likely a result of lower frequency of retrievals a these altitudes. Figure 15(b) shows the uncertainty of these drifts. Most of the drifts shown in Figure 15(a) are too small to estimated by the given data set, as shown in Figure 15(c), most of the points that passed the filter show a negative drift in the 0°-30° latitude range. Figure 15(d) shows the points from Figure 15(c) further filtered to exclude points where the drift is less than its uncertainty.

Figure 16(a) shows the results for modelling the VIS 1.2 data set with the deseasonalisation method. The spread of the linear drifts shown in Figure 16(a) looks similar to the spread shown in Figure 15(a), except here the drifts are generally negative at both poles. Many of the points in the polar region were not filtered out, and hardly any points were kept outside the polar region. This is similar to what was observed in Figure 13, where the same data was modelled using the deseasonalisation model.

Figure 17(a) shows the results for the VIS 3.13 data set. The general spread of the drifts looks different for this data set than what was observed for the version 1.2 data sets, and it looks similar to the spread seen when this data was modelled using the deseasonalisation method. Here, Figure 17 shows, in general, positive drifts at the polar latitudes at altitudes higher than around 50 km, with a negative drift around 50 km being observed globally. As previously discussed, the strong difference between measurements below 50 km and those above 50 km is likely a result of the measurement quality and infrequency of measurements above this altitude. Again, since this data set is much longer than the version 1.2 data set, Figure 17(b) shows drift uncertainties generally less than those shown in Figures 15(b) and 16(b).

Figures 23, 24, and 25 show the results of using the multilinear parametric trend model with the three data sets on a 5° latitudinal grid. From these results, it is evident how results from using the coarser grid were obtained. Interestingly, the uncertainties of the drifts are all at their highest at the northernmost and southernmost latitudes for each of these models; this is likely due to the presence of the polar vortex.

3.2.3 Comparing the methods

Figure 18 shows an example of an modelling version 3.13 VIS data for an (altitude, latitude) point, zoomed into the years from 2010-2017. The results of modelling the data using the deseasonalisation method (green) and the multilinear parametric trend model (red) are shown, along with just the linear part of the multilinear parametric trend model (blue). The data (the monthly averages of the ozone) is shown in black. On the residuals subplot, it is noticeable that the residual associated with just the linear term looks periodic; this demonstrates that introducing oscillatory terms should improve the model. For the two methods (green and red), there are sections on the plot where either is a better fit. The multilinear parametric trend model is expected to be more robust, but in this case it does not do a great job at representing the data. If the time series were longer (ie, if more data were available), perhaps it would be more apparent which model is more appropriate.

One simple step to improve the models, keeping the results in mind, would have been to work with a coarser resolution altitude grid. The altitude grid for all of the models in this study had a resolution of 0.5 km; by making the grid spacing wider more points would be included in each time series, making data sparseness less of an issue.

4 Next Steps

4.1 Quasi-biennial oscillation

In order to improve to parametric trend model used in this study, proxy data could be used to parametrize signals that are known to exist and have been measured. For example, the quasi-biennial oscillation (QBO) could be introduced using proxy data. The QBO is a quasiperiodic oscillation of the equatorial zonal wind in the tropical stratosphere with a period of approximately 28 or 29 months [16, 17]. By using proxy data, one can better estimate the signal in the ozone trends with around 28 or 29 month frequency (one would have to re-run the multilinear parametric trend model to no longer have the 28-month frequency terms since the proxy data would account for that signal).

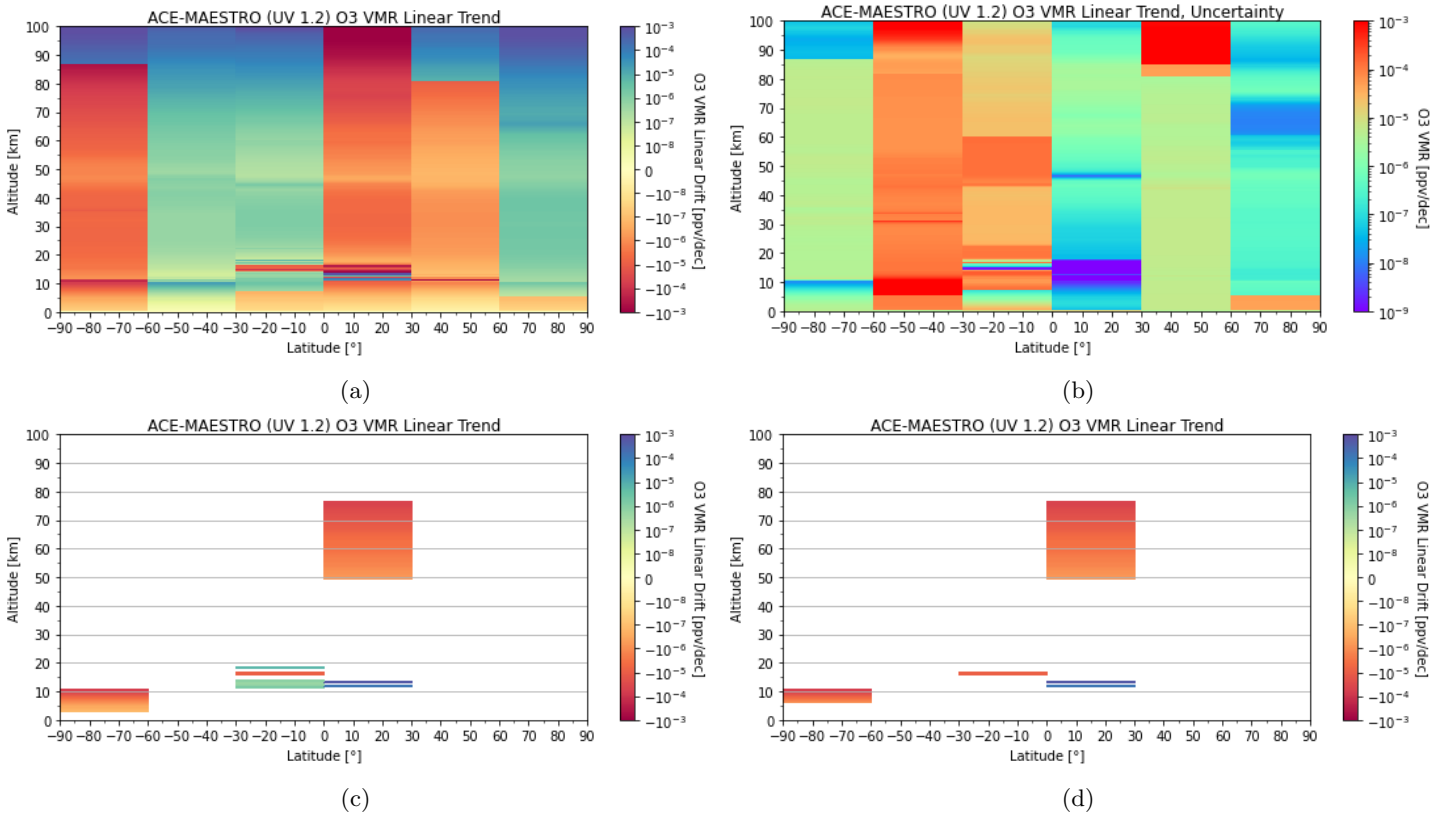

Figure 15: Results of modelling ACE-MAESTRO-UV 1.2 data from 2004-2011 using the mutlilinear parametric trend model. (a) shows the linear drift in ozone in [ppv/dec]; the uncertainties associated with (a) are shown in (b). (c) shows the result of filtering out points where $|\omega_0|_{min} \leq |\hat{\omega_0}|$ (where the estimated drift was found to be less than the minimum drift that could be estimated by the data set, found from equation 9). (d) shows the result of further filtering (c) to exclude points where the uncertainty of the drift was greater than the drift itself.

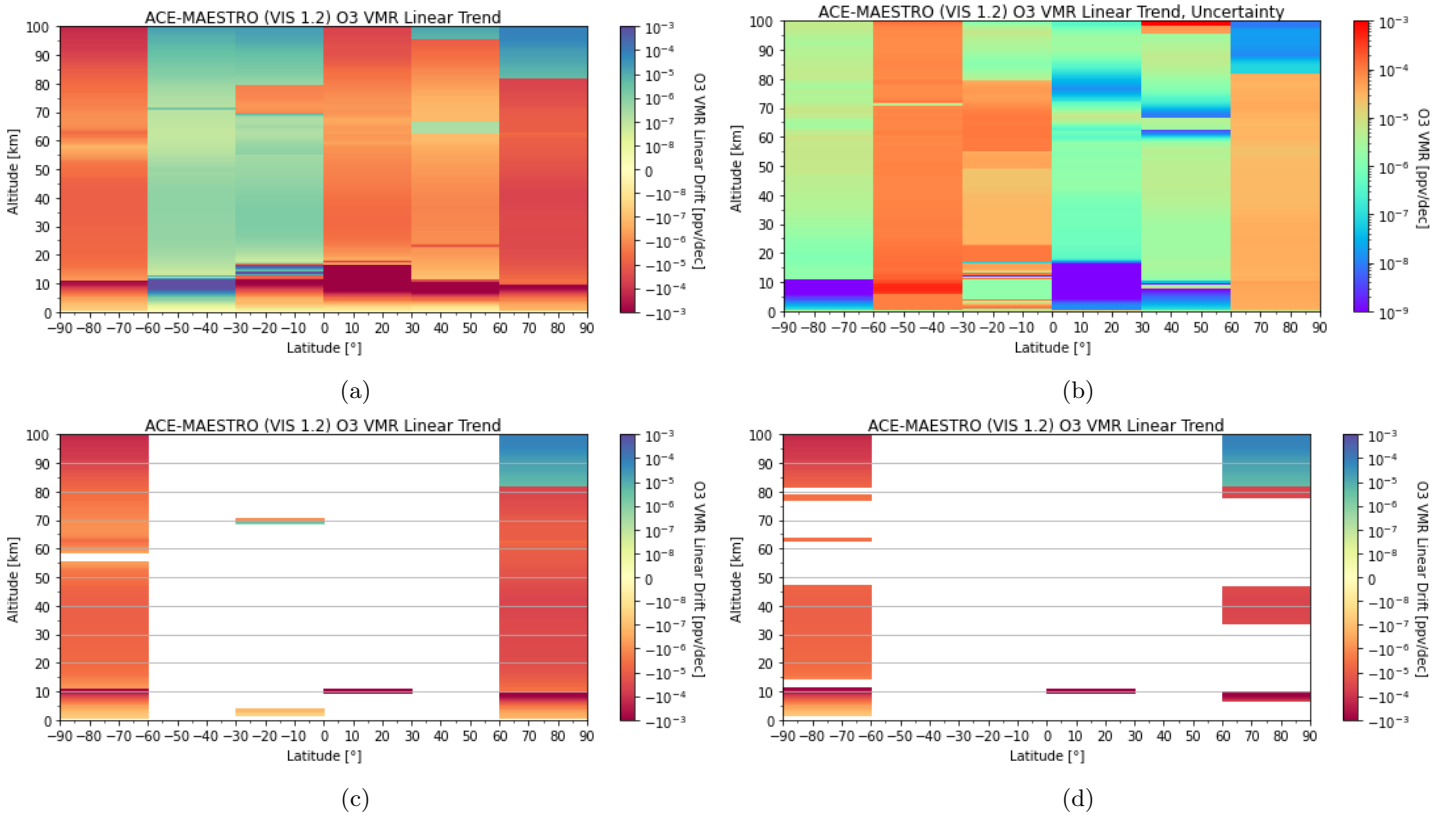

(a) (b)

(c) (d)

Figure 16: Same as Figure 15, but for ACE-MAESTRO-VIS 1.2 measurements from 2004-2011.

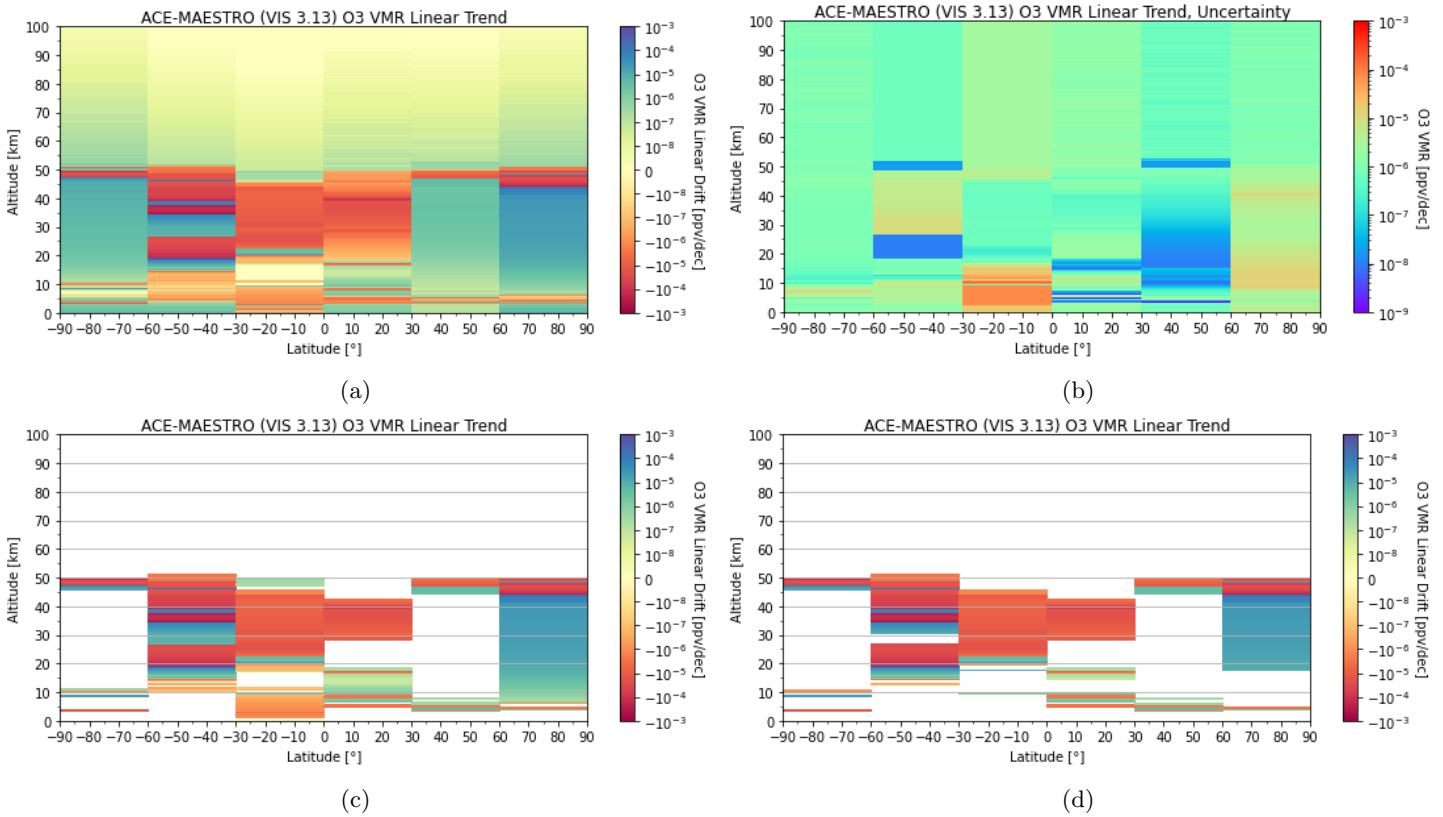

(a) (b)

(c) (d)

Figure 17: Same as Figure 15, but for ACE-MAESTRO-VIS 3.13 measurements from 2004-2020.

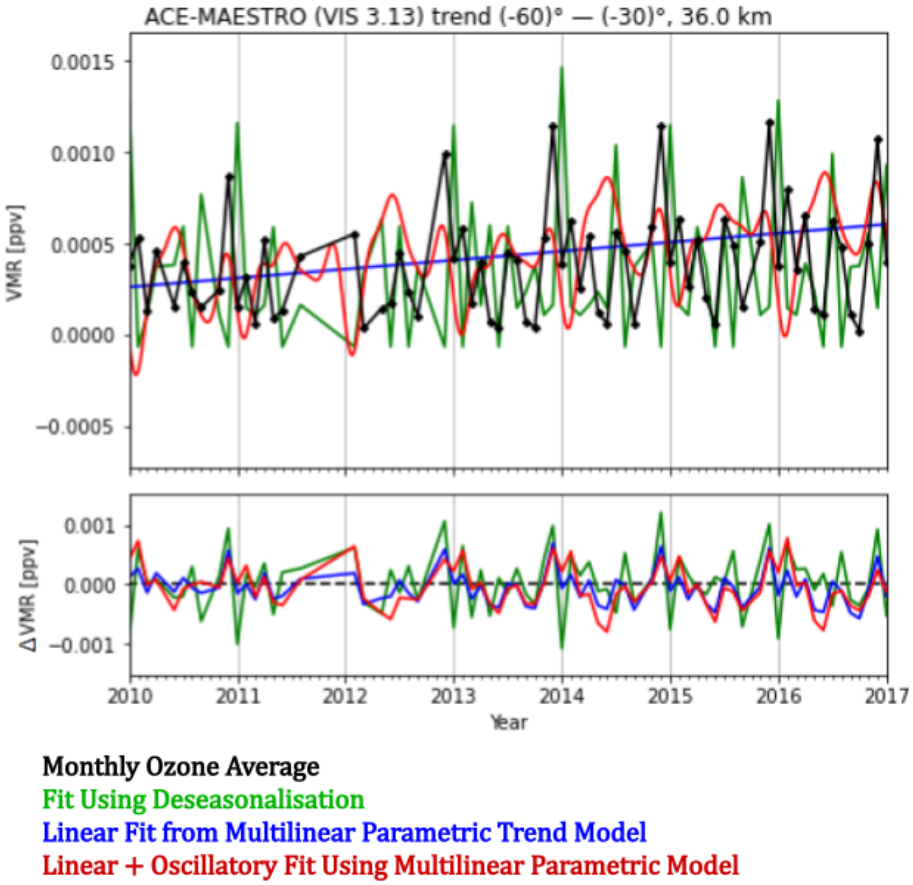

Figure 18: Different ways of modelling monthly average ozone at 60°S-30°S, 33.0 km altitude (zoomed in to 2010-2017). Below the models is a plot of the residuals for each fit.

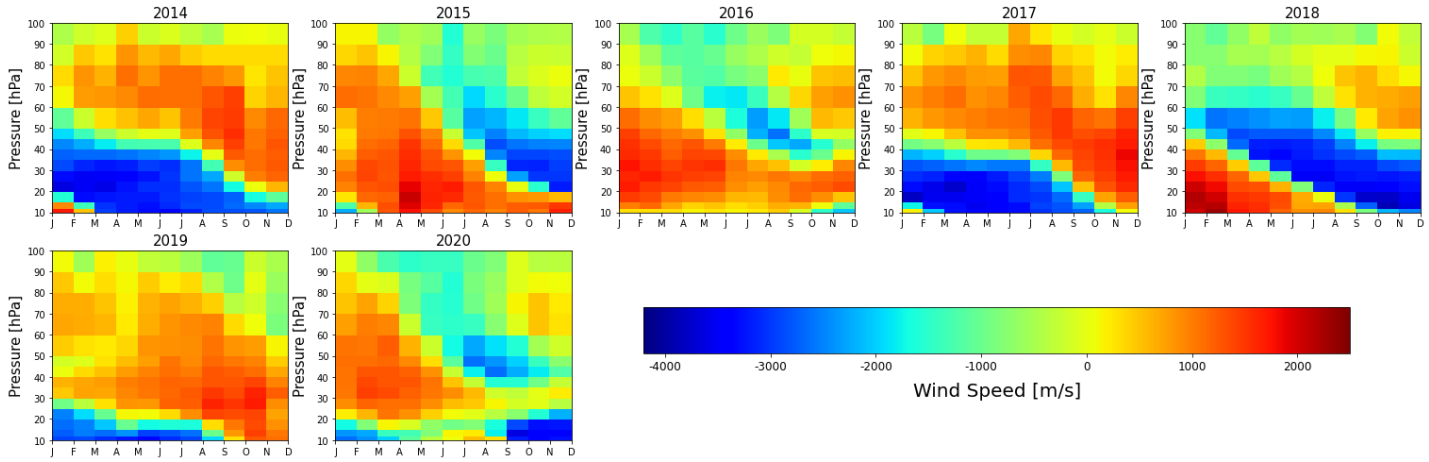

(a) Plot of monthly averaged winds at pressures 70, 50, 40, 30, 20, 15 and 10 hPa, from a radiosensor station in Singapore [18]. The 28-29 month frequency is very visible.

The quasi-biennial oscillation could be introduced by using Singapore winds at 30 and 50 hPa as a proxy, as was done in Eckert et al. [11, 18].

4.2 Instrumental drift

The ozone trends over time could be corrected by incorporating a term that accounts for ACE-MAESTRO's instrumental drift. Recall that the UV spectrometer was found to deteriorate since 2011, which is why no measurements from the UV spectrometer beyond 2011 were included in this study. Instrumental drift on a smaller magnitude could be accounted for by comparing measurements from ACE-MAESTRO with measurements from other instruments that measured the same air mass, and modelling how their differences changed over the years.

Some criteria for two measurements to have been of approximately the same air mass would be set, and these comparisons would be done between ACE-MAESTRO and a number of instruments.

The monthly average difference of measurements between ACE-MAESTRO with each instrument could be calculated, and the related time series could then fitted to a straight line, or with the same parametric trend model presented in von Clarmann et al. [10], resulting in a model of ACE-MAESTRO's instrumental drift. The drift model could then be subtracted from the model created in this study, producing a model of how atmospheric ozone changed in space and time, not as how ACE-MAESTRO observed it, but as it was. This method is based on considerations of instrumental drift in Bognar et al. [7], Eckert et al. [11], and Hubert et al. [19].

5 Conclusion

This report included a study ofatmospheric ozone in two parts: the first part to compare simultaneous measurements of ozone from ACE-MAESTRO's two spectrometers, and the second part was to model global ozone trends as seen by ACE-MAESTRO.

ACE-MAESTRO's version 1.2 UV and VIS and version 3.13 VIS data sets were compared. These comparisons were done pointwise as well as by profiles. They were also done yearly and cumulatively for the comparison period of 2004-2011. The availability of data from 0-10 and 80-100 km was particularly low. Measurements from the VIS spectrometer were generally smaller than those from the UV spectrometer. High uncertainties and low retrieval rates caused the comparisons in the 0-20 km and 60-100 km range to yield high differences.

The development of ozone in space and time was modelled using two different methods; this was done for each data set. Ozone quantities on a (altitude, latitude) grid were modelled as a linear drift with added oscillating components. The uncertainty of these models was high because of the limited data set, but in general, the results showed negative drifts in time in the middle latitudes and positive drifts elsewhere.

Next steps to this study could include improving upon the models used. For example, proxy data could be used to evaluate the QBO signal, or the instrumental drift could be accounted for.

6 Appendix A: Multilinear Parametric Trend Model

The following is a more detailed outline of the procedure discussed in section 3.2.2. The method is taken from von Clarmann et al. [10]. To model a data set $\boldsymbol{y(x)}$ as a straight line $\hat{\boldsymbol{y}} = a + b\boldsymbol{x}$ (ie, where ideally $\hat{\boldsymbol{y}} = \boldsymbol{y}$), one can use the following systems of equations. The covariance matrix of the dataset it denoted as $\boldsymbol{S}_y^{-1}$, and the vector $\boldsymbol{e}$ denotes a column of ones.

$$a = \frac{\boldsymbol{x}^T\boldsymbol{S}_y^{-1}\boldsymbol{y} - \boldsymbol{e}^T\boldsymbol{S}_y^{-1}\boldsymbol{x}b}{\boldsymbol{e}^T\boldsymbol{S}_y^{-1}\boldsymbol{e}} \tag{10}$$

$$b = \frac{\boldsymbol{x}^T\boldsymbol{S}_y^{-1}\boldsymbol{y}\boldsymbol{e}^T\boldsymbol{S}_y^{-1}\boldsymbol{e} - \boldsymbol{x}^T\boldsymbol{S}_y^{-1}\boldsymbol{e}\boldsymbol{e}^T\boldsymbol{S}_y^{-1}\boldsymbol{y}}{\boldsymbol{x}^T\boldsymbol{S}_y^{-1}\boldsymbol{x}\boldsymbol{e}^T\boldsymbol{S}_y^{-1}\boldsymbol{e} - \boldsymbol{x}^T\boldsymbol{S}_y^{-1}\boldsymbol{e}\boldsymbol{e}^T\boldsymbol{S}_y^{-1}\boldsymbol{x}} \tag{11}$$

The uncertainties of these parameters is shown below:

$$\sigma_a = \left(\frac{\boldsymbol{x}^T\boldsymbol{S}_y^{-1}\boldsymbol{x}\boldsymbol{e}^T\boldsymbol{S}_y^{-1} - \boldsymbol{x}^T\boldsymbol{S}_y^{-1}\boldsymbol{x}\boldsymbol{x}^T\boldsymbol{S}_y^{-1}}{\boldsymbol{e}^T\boldsymbol{S}_y^{-1}\boldsymbol{e}\boldsymbol{x}^T\boldsymbol{S}_y^{-1} - \boldsymbol{x}^T\boldsymbol{S}_y^{-1}\boldsymbol{x}\boldsymbol{x}^T\boldsymbol{S}_y^{-1}x}\right)\boldsymbol{S}_y\left(\frac{\boldsymbol{x}^T\boldsymbol{S}_y^{-1}\boldsymbol{x}\boldsymbol{e}^T\boldsymbol{S}_y^{-1} - \boldsymbol{x}^T\boldsymbol{S}_y^{-1}\boldsymbol{x}\boldsymbol{x}^T\boldsymbol{S}_y^{-1}}{\boldsymbol{e}^T\boldsymbol{S}_y^{-1}\boldsymbol{e}\boldsymbol{x}^T\boldsymbol{S}_y^{-1} - \boldsymbol{x}^T\boldsymbol{S}_y^{-1}\boldsymbol{x}\boldsymbol{x}^T\boldsymbol{S}_y^{-1}x}\right)^T \tag{12}$$

$$\sigma_b = \left(\frac{\boldsymbol{e}^T\boldsymbol{S}_y^{-1}\boldsymbol{e}\boldsymbol{x}^T\boldsymbol{S}_y^{-1} - \boldsymbol{x}^T\boldsymbol{S}_y^{-1}\boldsymbol{e}\boldsymbol{e}^T\boldsymbol{S}_y^{-1}}{\boldsymbol{x}^T\boldsymbol{S}_y^{-1}\boldsymbol{x}\boldsymbol{e}^T\boldsymbol{S}_y^{-1}\boldsymbol{e} - \boldsymbol{x}^T\boldsymbol{S}_y^{-1}\boldsymbol{e}\boldsymbol{e}^T\boldsymbol{S}_y^{-1}x}\right)\boldsymbol{S}_y\left(\frac{\boldsymbol{e}^T\boldsymbol{S}_y^{-1}\boldsymbol{e}\boldsymbol{x}^T\boldsymbol{S}_y^{-1} - \boldsymbol{x}^T\boldsymbol{S}_y^{-1}\boldsymbol{e}\boldsymbol{e}^T\boldsymbol{S}_y^{-1}}{\boldsymbol{x}^T\boldsymbol{S}_y^{-1}\boldsymbol{x}\boldsymbol{e}^T\boldsymbol{S}_y^{-1}\boldsymbol{e} - \boldsymbol{x}^T\boldsymbol{S}_y^{-1}\boldsymbol{e}\boldsymbol{e}^T\boldsymbol{S}_y^{-1}x}\right)^T \tag{13}$$

The model can be corrected to include periodic terms of frequencies $2\pi/l_i$ (where l_i is an integer number of months):

$$\hat{\boldsymbol{y}} = a + b\boldsymbol{x} + \sum_i \left(c_i sin(\frac{2\pi\boldsymbol{x}}{l_i}) + d_i cos(\frac{2\pi\boldsymbol{x}}{l_i})\right) \tag{14}$$

The solve this system, the following equations are used (to illustrate the model, only one c and d parameter is used, but the matrices can be extended for any number of sinusoidal terms):

$$\boldsymbol{T}\begin{bmatrix} a \\ b \\ c \\ d \end{bmatrix} = \boldsymbol{q} \tag{15}$$

such that:

$$T_{1,1} = 2\boldsymbol{e}^T\boldsymbol{S}_y^{-1}\boldsymbol{e}$$

$$T_{1,2} = 2\boldsymbol{e}^T\boldsymbol{S}_y^{-1}\boldsymbol{x}$$

$$\vdots$$

$$T_{4,4} = 2\boldsymbol{v}_{cos}^T\boldsymbol{S}_y^{-1}\boldsymbol{v}_{cos}$$

(where $\boldsymbol{v}_{cos} = cos(2\pi\boldsymbol{x}/l)$), and:

$$q_1 = 2\boldsymbol{e}^T\boldsymbol{S}_y^{-1}\boldsymbol{y}(\boldsymbol{x})$$

$$\vdots$$

$$q_4 = 2\boldsymbol{v}_{cos}^T\boldsymbol{S}_y^{-1}\boldsymbol{y}(\boldsymbol{x})$$

The covariance matrix of the parameters for this model can be found as follows:

$$\boldsymbol{S}_{a,b,c,d} = \left(\boldsymbol{T}^{-1}\begin{bmatrix} 2\boldsymbol{e}^T\boldsymbol{S}_y^{-1} \\ 2\boldsymbol{x}^T\boldsymbol{S}_y^{-1} \\ 2\boldsymbol{v}_{sin}^T\boldsymbol{S}_y^{-1} \\ 2\boldsymbol{v}_{sin}^T\boldsymbol{S}_y^{-1} \end{bmatrix}\right)\boldsymbol{S}_y\left(\boldsymbol{T}^{-1}\begin{bmatrix} 2\boldsymbol{e}^T\boldsymbol{S}_y^{-1} \\ 2\boldsymbol{x}^T\boldsymbol{S}_y^{-1} \\ 2\boldsymbol{v}_{sin}^T\boldsymbol{S}_y^{-1} \\ 2\boldsymbol{v}_{sin}^T\boldsymbol{S}_y^{-1} \end{bmatrix}\right)^T \tag{16}$$

7 Appendix B: Figures

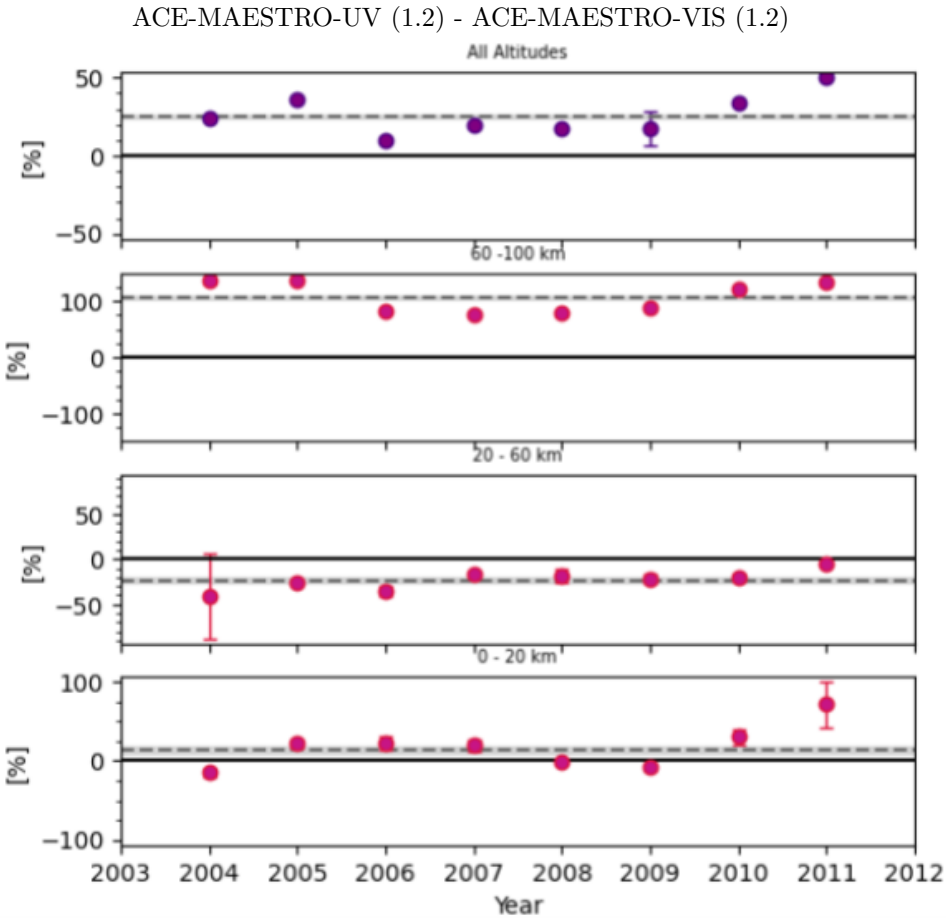

Figure 20: Time series of mean relative differences between ACE-MAESTRO UV 1.2 and VIS 1.2 measurements, over 3 altitude ranges as well as over the complete altitude range (0-100 km).

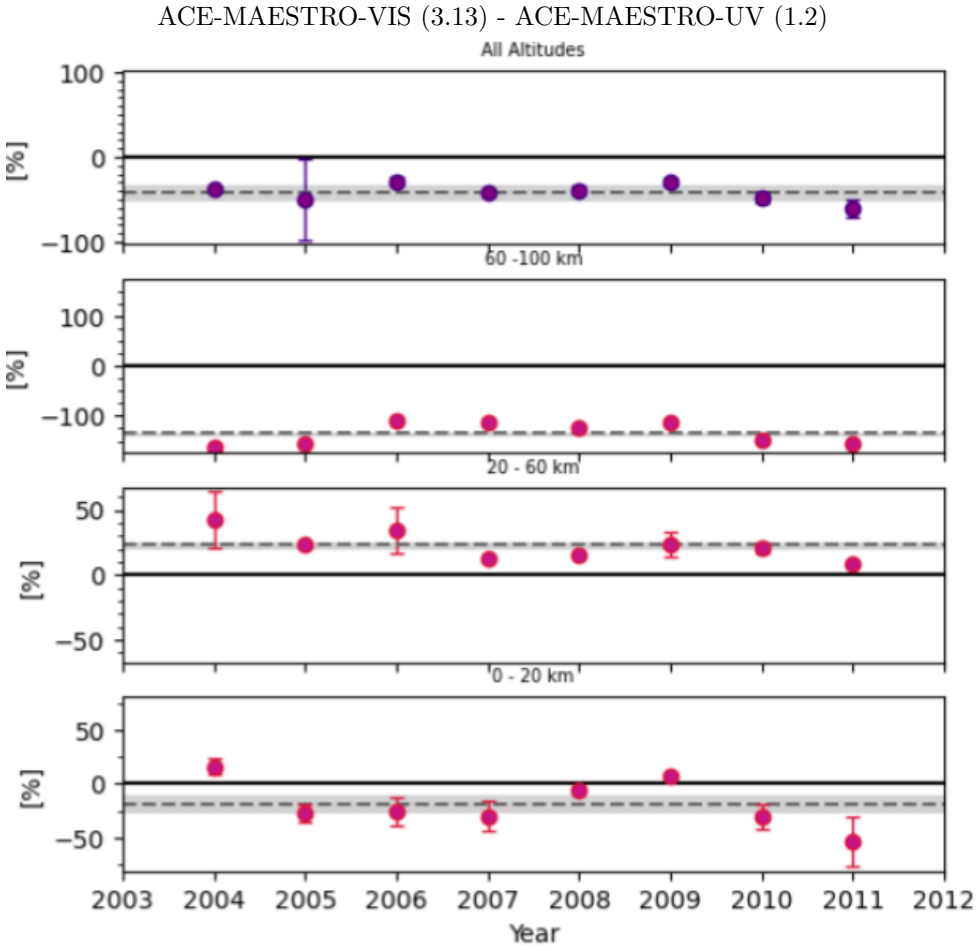

Figure 21: Time series of mean relative differences between ACE-MAESTRO VIS 3.13 and UV 1.2 measurements, over 3 altitude ranges as well as over the complete altitude range (0-100 km).

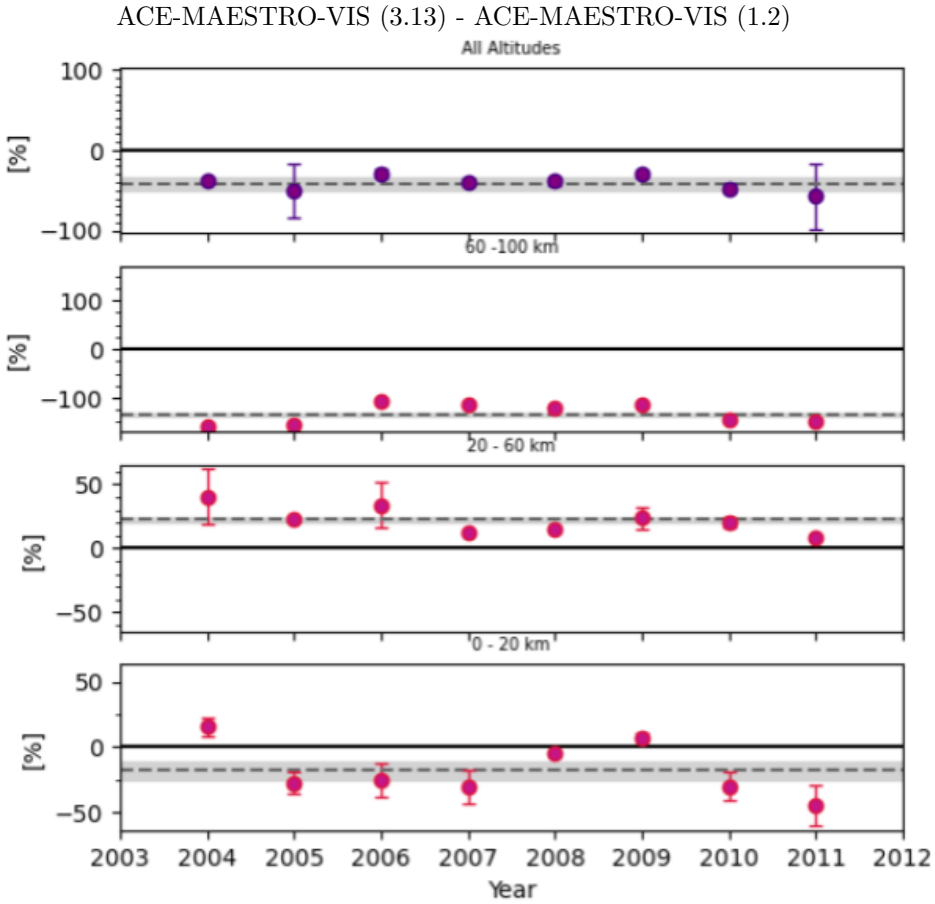

Figure 22: Time series of mean relative differences between ACE-MAESTRO VIS 3.13 and VIS 1.2 measurements, over 3 altitude ranges as well as over the complete altitude range (0-100 km).

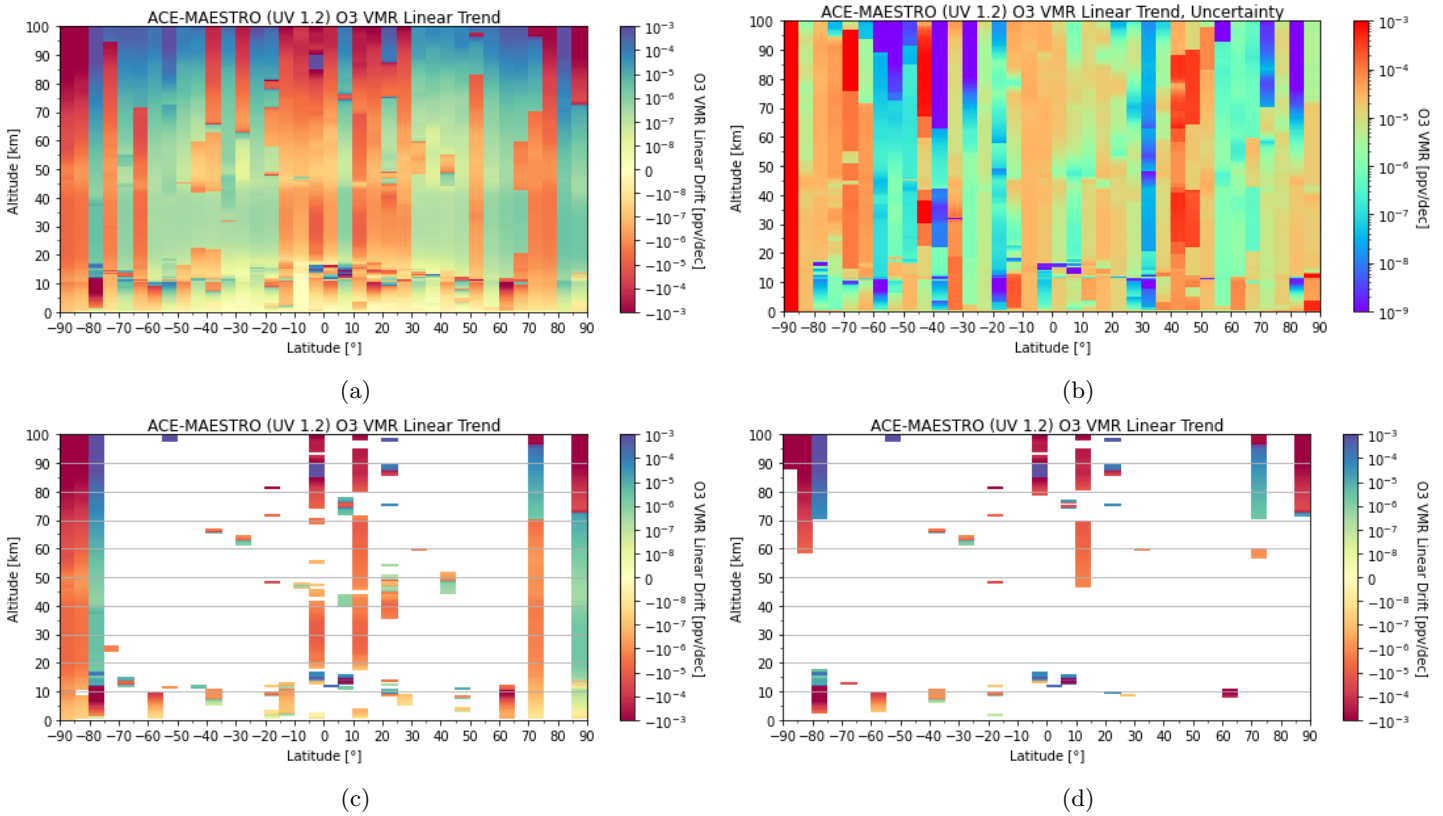

(a) (b)

(c) (d)

Figure 23: Same as Figure 15, but on a 5° resolution latitudinal grid.

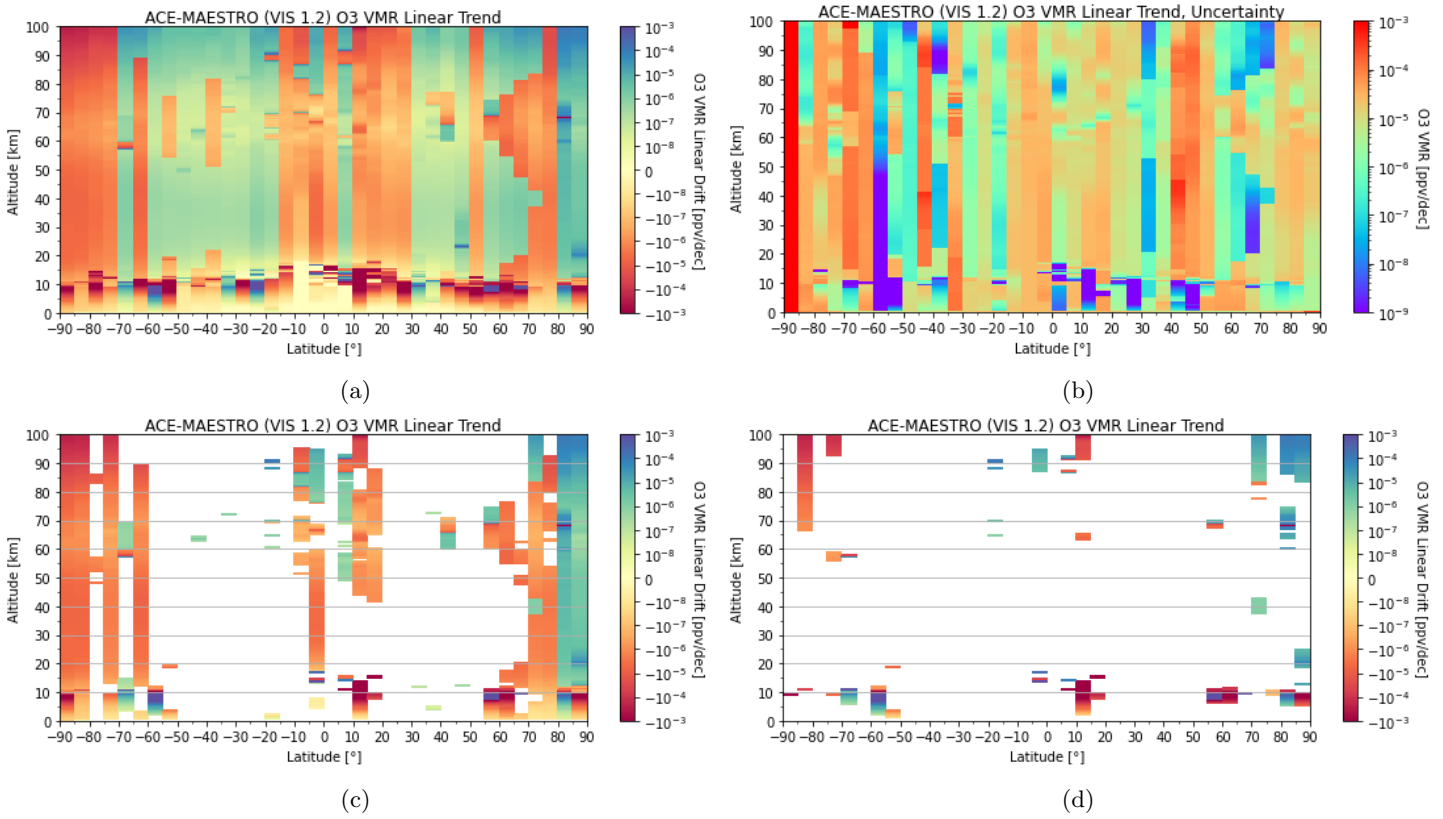

(a) (b)

(c) (d)

Figure 24: Same as Figure 16, but on a 5° resolution latitudinal grid.

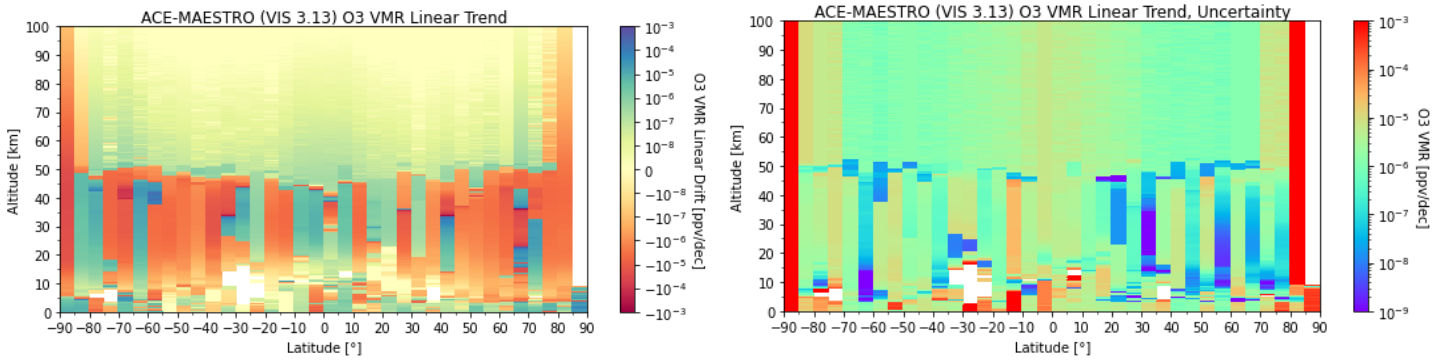

(a)

(b)

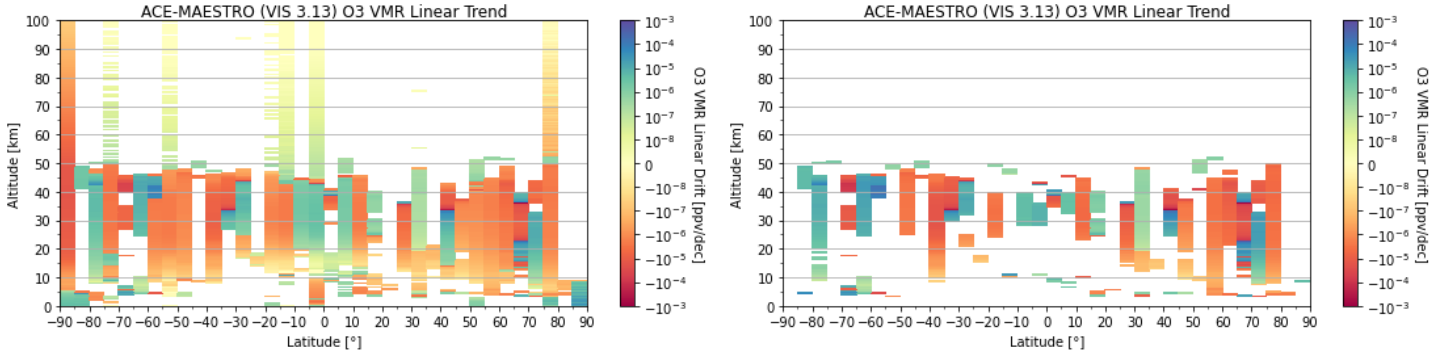

(c)

(d)

Figure 25: Same as Figure 17, but on a 5° resolution latitudinal grid.

8 References

1. C. T. Mcelroy, C. R. Nowlan, J. R. Drummond, P. F. Bernath, et. al., "The ACE-MAESTRO instrument on SCISAT: description, performance, and preliminary results," Applied Optics, vol. 46, no. 20, p. 4341, 2007.

2. P. F. Bernath, C. T. McElroy, M. C. Abrams, C. D. Boone, et. al., "Atmospheric Chemistry Experiment (ACE): mission overview," Geophys. Res. Lett., 2005

3. "Solar Occultation," Solar Occultation - Atmospheric Chemistry Experiment. [Online].
   Available: http://www.ace.uwaterloo.ca/solaroccultation.php.

4. "Slant Column and Vertical Column Densities," SCD vs. VCD. [Online]. Available: https://sacs.aeronomie.be/info/scdvcd.php.

5. J. Zou, "ACE-MAESTRO Data Version 1.2," 2006.

6. J. Zou, J. Drummond, T. McElroy, "ACE-MAESTRO Level 2 Version 3.13 Data Description and File Formats", 2018.

7. K. Bognar, X. Zhao, K. Strong, C. Boone, et. al, "Updated validation of ACE and OSIRIS ozone and NO2 measurements in the Arctic using ground-based instruments at Eureka, Canada," Journal of Quantitative Spectroscopy and Radiative Transfer, vol. 238, p. 106571, 2019.

8. E. Dupuy, K. A. Walker, J. Kar, C. D. Boone, et al. "Validation of ozone measurements from the Atmospheric Chemistry Experiment (ACE)", Atmospheric Chemistry and Physics, vol. 9, pp. 287-343, 2009.

9. J. Kar, C. T. Mcelroy, J. R. Drummond, J. Zou, et. al., "Initial comparison of ozone and NO2profiles from ACE-MAESTRO with balloon and satellite data," Journal of Geophysical Research, vol. 112, no. D16, 2007.

10. T. V. Clarmann, G. Stiller, U. Grabowski, E. Eckert, et al., "Technical Note: Trend estimation from irregularly sampled, correlated data," Atmospheric Chemistry and Physics, vol. 10, no. 14, pp. 6737–6747, 2010.

11. E. Eckert, T. V. Clarmann, M. Kiefer, G. P. Stiller, et. al., "Drift-corrected trends and periodic variations in MIPAS IMK/IAA ozone measurements," Atmospheric Chemistry and Physics, vol. 14, no. 5, pp. 2571–2589, 2014.

12. E. C. Weatherhead, G. C. Reinsel, G. C. Tiao, X. Meng, et. al., "Factors affecting the detection of trends: Statistical considerations and applications to environmental data", Journal of Geophysical Research, vlol. 103, no. D14, pp. 17,149-17,161, 1998. .

13. J. R. Norris, R. J. Allen, A. T. Evan, M. D. Zelinka, C. W. O'Dell, and S. A. Klein, "Evidence for climate change in the satellite cloud record," Nature, vol. 536, no. 7614, pp. 72–75, 2016.

14. F. G. L. Cawkwell, J. L. Bamber, and J.-P. Muller, "Determination of cloud top amount and altitude at high latitudes," Geophysical Research Letters, vol. 28, no. 9, pp. 1675–1678, 2001.

15. "Cloud Heights at Different Latitudes," Cloud Heights by Latitude - Windows to the Universe. [Online]. Available: https://www.windows2universe.org/earth/Atmosphere/clouds/heights_latitude.html.

16. "The Quasi-biennial Oscillation (QBO)," NASA. [Online]. Available: https://acd-ext.gsfc.nasa.gov/Data-services/met/qbo/qbo.html.

17. M. P. Baldwin, L. J. Grey, T. J. Dunkerton, et al., "THE QUASI-BIENNIAL OSCILLATION," Reviews of Geophysics, vol. 39, no. 2, pp. 179–229, May 2001.

18. "QBO," QBO • Atmosphärendynamik •, 12-Feb-2007. [Online]. Available: https://www.geo.fu-berlin.de/-met/ag/strat/produkte/qbo.

19. D. Hubert, J.C. Lambert, T. Verhoelst, J. Granville, et. al., "Ground-based assessment of the bias and long-term stability of 14 limb and occultation ozone profile data records," Atmospheric Measurement Techniques, vol. 9, no. 6, pp. 2497–2534, 2016.

20. D. G. Dufour, J. R. Drummond, C. T. Mcelroy, C. Midwinter, et. al., "Intercomparison of Simultaneously Obtained Infrared (4.8 m) and Visible (515715 nm) Ozone Spectra Using ACE-FTS and MAESTRO," The Journal of Physical Chemistry A, vol. 109, no. 39, pp. 8760–8764, 2005.

21. B. Efron and R. Tibshirani, "[Bootstrap Methods for Standard Errors, Confidence Intervals, and Other Measures of Statistical Accuracy]: Rejoinder," Statistical Science, vol. 1, no. 1, pp. 54–75, 1986.

22. J. O. Street, R. J. Carroll, and D. Ruppert, "A Note on Computing Robust Regression Estimates Via Iteratively Reweighted Least Squares," The American Statistician, vol. 42, no. 2, p. 152, 1988.